NRF2 shortage in human skin fibroblasts dysregulates matrisome gene expression and affects collagen fibrillogenesis

Mélanie Salamito, Benjamin Gillet, Delfien Syx, Elisabeth Vaganay, Marilyne Malbouyres, Catherine Cerutti, Nicolas Tissot, Chloé Exbrayat-Heritier, Philippe Perez, Christophe Jones, et al.

NRF2 shortage in human skin fibroblasts dysregulates matrisome gene expression and affects collagen fibrillogenesis

Mélanie Salamito[1,2], Benjamin Gillet[1], Delfien Syx[3], Elisabeth Vaganay[1], Marilyne Malbouyres[1], Catherine Cerutti[1], Nicolas Tissot[2], Chloé Exbrayat-Heritier[1], Philippe Perez[2], Christophe Jones[2], Sandrine Hughes[1], Fransiska Malfait[3], Valérie Haydont[2], Sibylle Jäger[2] and Florence Ruggiero[1#]

[1] Université de Lyon, ENSL, CNRS, Institut de Génomique Fonctionnelle de Lyon (IGFL), Université Claude Bernard Lyon 1, Lyon, France

[2] L'Oréal Research and Innovation, Aulnay-sous-Bois, France

[3] Department of Biomolecular Medicine, Center for Medical Genetics, Ghent University and Ghent University Hospital, Ghent, Belgium

[#]corresponding author: Florence Ruggiero, Institut de Génomique Fonctionnelle de Lyon (IGFL) – ENS de Lyon, 46 Allée d'Italie, F69364 Lyon cedex 07, France; Phone number: +33 (0)4 72 72 26 57; Fax number: +33 (0)4 72 72 26 02; E-mail: florence.ruggiero@ens-lyon.fr; Twitter account @TheRuggieroLab

Short Title: NRF2 shortage impacts human dermis matrisome

Abbreviations: AFM, Atomic Force Microscopy; BCS, Brittle Cornea Syndrome; ECM, Extra-Cellular Matrix; HDF, Human Dermal papillary Fibroblasts; NT, Non-Transfected; NRF2, nuclear factor E2-related factor; SHG, Second Harmonic Generation microscopy; ROS, Reactive Oxygen Species; shRNA, short hairpin RNA; siCtrl small interfering RNA control; siRNA, small interfering RNA; TEM, Transmission Electron Microscopy

ABSTRACT

NRF2 is a master regulator of anti-oxidative response that was recently proposed as a potential regulator of extracellular matrix (ECM) gene expression. Fibroblasts are major ECM producers in all connective tissues including dermis. A better understanding of NRF2-mediated ECM regulation in skin fibroblasts is thus of great interest for skin homeostasis maintenance and aging protection. Here, we investigate the impact of NRF2 downregulation on matrisome gene expression and ECM deposits in human primary dermal fibroblasts. RNA-seq-based transcriptome analysis of NRF2 silenced dermal fibroblasts shows that ECM genes are the most regulated gene sets, highlighting the relevance of the NRF2-mediated matrisome program in these cells. Using complementary light and electron microscopy methods, we show that NRF2 deprivation in dermal fibroblasts results in reduced collagen I biosynthesis and impacts collagen fibril deposition. Moreover, we identify ZNF469, a putative transcriptional regulator of collagen biosynthesis, as a novel target of NRF2. Both ZNF469 silenced fibroblasts and fibroblasts derived from Brittle Corneal Syndrome patients carrying mutations in *ZNF469* show reduced collagen I gene expression. Our study shows that NRF2 orchestrates matrisome expression in human skin fibroblasts through direct or indirect transcriptional mechanisms that could be prioritized to target dermal ECM homeostasis in health and disease.

INTRODUCTION

Skin fibroblasts that constitute the main cell type are chiefly responsible for biosynthesis and deposition of the dermal extracellular matrix (ECM). Dermal ECM represents a highly dynamic structure that undergoes constant remodeling (Nyström and Bruckner-Tuderman, 2019). Its compacted structure resists tension, shear and compression. Besides its critical role in the biomechanical properties of the skin, ECM regulates fundamental cell functions, such as cell proliferation, migration and differentiation (Frantz et al., 2010). As such, dysregulation or alteration of the ECM can lead to numerous pathologies including cancers and fibrosis (Taha and Naba, 2019; Theocharis et al., 2019). Structural changes in the dermal ECM are also the prime cause of skin aging signs (Haydont et al., 2019a; Sparavigna, 2020). The proper regulation of the dermal ECM is thus paramount for skin homeostasis maintenance and extensive investigations have been undertaken to identify the contributing factors (Statzer et al., 2021). Recently, the nuclear factor E2-related factor (NRF2) emerged as an ECM regulator: 1) In *C. elegans*, SKN1, the worm ortholog of NRF2 promoted *C. elegans* longevity through transcriptional positive regulation of collagen genes under specific metabolic conditions (Ewald et al., 2015); 2) The genetic upregulation of NRF2 in mice changed structural ECM gene expression (Hiebert et al., 2018), suggesting a conserved role of SKN-1/NRF2 in mammals.

NRF2 is a master regulator of the intracellular antioxidant response and xenobiotic metabolism (Hayes and Dinkova-Kostova, 2014; Tonelli et al., 2018). Under oxidative or xenobiotic stress-conditions, reactive oxygen species (ROS) and electrophiles induce a conformational change of its repressor Kelch-like ECH-associating protein 1 (KEAP1) that disrupts its binding to NRF2. NRF2 can then translocate to the nucleus and initiate transcription of its target genes (Suzuki et al., 2019). The complexity of the NRF2 pathway is illustrated by its hundreds of target genes. Among them are genes involved in the antioxidant glutathione (GSH)

homeostasis, ROS and xenobiotic detoxification, and heme and iron metabolism (Huang et al., 2015; Dodson et al., 2019).

In skin, NRF2 is known to protect resident cells from UV or pollution induced oxidative stress (Schäfer et al., 2010; Gęgotek and Skrzydlewska, 2015; Marrot, 2018). NRF2 is also involved in the wound healing process and in the skin immune response, by clearing oxidative stress and inflammation (Kobayashi et al., 2016; Ambrozova et al., 2017; Hiebert and Werner, 2019). NRF2 activation improves skin conditions as psoriasis and systemic sclerosis (SSc) (Brück et al., 2018; Kavian et al., 2018; Wu et al., 2020). Decreased NRF2 signaling contributes to the aging process in several tissues (Bruns et al., 2015; Zhang et al., 2015; Schmidlin et al., 2019). In the present study, we downregulated NRF2 expression under non-oxidative conditions in human dermal papillary fibroblasts (HDF) to investigate the impact of NRF2 deprivation on matrisome expression and ECM organization in the extracellular space. We demonstrate that knockdown of NRF2 in HDF altered the ECM gene expression profile. NRF2 controls collagen I expression levels and collagen fibrillogenesis, thus ECM structure and properties, possibly through the identified NRF2 target, ZNF469, a factor involved in a connective tissue disease associated with collagen fibrillogenesis deficiency.

RESULTS

Unbiased transcriptomic profiling of HDF silenced for NRF2

To investigate the potential role of NRF2 in primary HDF we decided to perform an unbiased transcriptomic analysis using siRNA targeting NRF2. Papillary fibroblasts were chosen for their higher proliferation rate and biosynthetic activity than reticular fibroblasts (Nauroy et al., 2017). We opted for an RNA interference strategy to mimic the decrease of NRF2 signaling observed in aged tissues.

Papillary fibroblasts derived from young female donors were transfected with two different siRNAs targeting NRF2 (siNrf2_1 and siNrf2_2). As reduced expression of NRF2 can lead to cell oxidative stress-associated cell death we verified that the HDF did not exhibit any morphological sign of stress (supplementary Figure S1a). The downregulation of *NFE2L2* and its targets *NQO1* and *SLC7A11* was assessed using RT-qPCR and confirmed at the protein level (NRF2, SLC7A11*)* (supplementary Figure S1b-c).

Principal component analysis (PCA) of the RNA-sequencing data showed that, despite the important donor effect, the values nicely cluster by condition when plotted on the PC3 and PC4 axes, that account for 15% of the total variance (supplementary Figure S2a). Importantly, the control conditions (NT, non-transfected; siRNA control, siCtrl) clustered together (PC3/PC4 axes) and bioinformatics analysis did not reveal any significantly differentially expressed genes between the two conditions excluding experimental bias due to transfection stress.

Hundreds of genes were significantly differentially expressed in siNrf2 fibroblasts compared to siCtrl. We identified respectively 410 and 550 differentially expressed genes in siNrf2_1 and siNrf2_2 cells compared to controls (Figure 1a). About 10% of those genes were NRF2 conventional targets, its detoxification target genes*,* and genes involved in heme and iron metabolism or proteostasis (supplementary Figure S2b-d; supplementary Table S1).

As oxidative stress was reported to affect ECM gene expression (Avantaggiato et al., 2014; Spadoni et al., 2015), ROS levels were measured in our samples that exclude redox imbalance due to possible transfection stress (supplementary Figure S3a). In addition, RNA-seq expression levels of known ROS-induced genes *SOD1*, *SOD2*, *SOD3* (encoding super oxide dismutases) and *NOX4* (NADPH oxidase 4) (St-Pierre et al., 2006; Murphy-Marshman et al., 2017), were unchanged in all conditions (supplementary Figure S3b). To conclude, NRF2 silencing in HDF was effective and our results were not skewed by indirect effects.

NRF2 knockdown specifically affects matrisome gene-expression profile in HDF

An expanded view of the ECM is to analyze changes in expression of genes defined as the "tissue skeleton" (Haydont et al., 2019b). The "ECM" and "secreted factors" categories overlap with matrisome categories (Naba et al., 2012) (Figure 1a-b). The "tissue skeleton" genes respectively represented 29% and 35% in siNrf2_1 and siNrf2_2 fibroblasts compared to controls (Figure 1a). Among the "tissue skeleton" categories, the matrisome-related "ECM" and "secreted factors" gene sets were collectively the most dysregulated gene sets (about 30%) (Figure 1b). Besides, the highly represented "focal adhesion" and "cytoskeleton" categories indicated that changes in ECM gene expression may impact HDF behavior.

Next, we detailed specifically the matrisome gene expression profile of siNrf2 fibroblasts and identified "core matrisome", "secreted factors", and "ECM regulators" gene categories as the most significantly impacted by NRF2 silencing (Figure 1a). Relevantly, both siNrf2 displayed similar distribution of matrisome gene categories, albeit differences in gene subsets. To even out potential variability in the regulation of gene expression levels between the two siRNAs, we lowered the fold change threshold to 1.4 (adjusted p-value <0.05). In doing so, we identified 37 commonly differentially expressed genes (supplementary Table S2) among which 13 core matrisome genes (Figure 1c).

As ECMs are made of protein networks that are critical for their function we then analyzed the molecular links between the 37 encoded proteins using the STRING database (Figure 1d). This revealed a major hub made of both core matrisome proteins, including collagens I (*COL1A1*, *COL1A2)*, X (*COL10A1)* and XXIV (*COL24A1*), elastic fibril components (*ELN* and *FBN2),* and ECM regulators (*TGM2* and *COMP*). Two additional smaller hubs were composed of secreted factors (one related to inflammation or the second containing growth factors) (Figure 1d). Most of the collagens were downregulated including the fibroblast markers *COL1A1* and

COL1A2 whereas elastin (*ELN*), periostin (*POSTN*) and cartilage oligomeric protein (*COMP*) were upregulated. Altogether, we conclude that ECM genes are *bona fide* NRF2 targets in HDF.

NRF2 silencing alters collagen fibril diameter and organization by decreasing collagen I expression

We next explored the impact of NRF2 silencing on the ECM at the protein level. Production and deposition of substantial amount of ECM by cells require several days of culture, technically not achievable with transient infection. We therefore established primary HDF lines with stable NRF2 silencing by lentivirus-mediated infection (shNrf2) (supplementary Figure S4). Decrease of the conventional redox targets *NQO1* and *SLC7A11* confirmed that NRF2 activity was efficiently blunted (supplementary Figure S4d-e).

We used Second Harmonic Generation (SHG) microscopy to visualize collagen fibers produced by shNrf2 fibroblasts after 8 days of culture. SHG microscopy allows imaging well-formed collagen fibers of sufficient diameter (>30nm) without any labeling, on a large field of view (Bancelin et al., 2012; 2015). A higher signal indicates either a greater abundance of fibrillar collagen and/or a denser and less isotropic organization of the fibrils. SHG images of shNrf2 showed a substantial decrease in fluorescence compared to controls indicating that NRF2 knockdown perturbed collagen fibril formation in HDF (Figure 2a).

Transmission electron microscopy (TEM) confirmed that shNrf2 collagen fibrils are thinner with a barely visible banded pattern and revealed numerous patches of disorganized unidentified ECM components (Figure 2b). In contrast, shCtrl fibroblasts ECM showed striated large collagen fibrils interspaced with filamentous ECM proteins and decorated with electron-dense proteoglycan-like aggregates (Figure 2b). Quantification confirmed that the mean of shNrf2 fibril diameters is significantly smaller than those of shCtrl (17.50±0.23 nm and 23.46±0.61 nm, respectively) (Figure 2c). Collagen fibril distribution patterns indicated a

predominance of regular narrow-diameter fibrils peaking at 14-18 nm in shNrf2 samples with no fibrils of a diameter > 25 nm, whereas shCtrl fibrils were heterogenous and displayed a wider range of fibril diameters (10-50 nm) (Figure 2d). Hence, the expression level of NRF2 influenced the collagen fibril network by decreasing the diameter of individual fibrils. We concluded that NRF2 knockdown in HDF results in a dysfunctional regulation of the formation and lateral growth of collagen fibers.

As changes in collagen fibril diameter can affect ECM rigidity, we used atomic force microscopy (AFM) to measure the mechanical properties of decellularized shCtrl versus shNrf2 samples. AFM images identified differences in ECM density between shCtrl and shNrf2 samples that confirm that shNrf2 fibroblasts produced fewer collagen fibrils than controls; However, significant change in ECM rigidity was not observed (supplementary Figure S5).

The diameter of heterotypic collagen fibrils correlates with the collagen I/V ratio (Ricard-Blum and Ruggiero, 2005). Gene expression of *COL1A1* and *COL1A2* was significantly decreased in shNrf2 whereas expression of *COL5A1* remained unchanged (Figure 3a). For validation at the protein level, we next performed immunofluorescence staining of shNrf2 and shCtrl fibroblasts cultivated in presence (referred to as intra+extracellular staining) or absence (referred to as intracellular staining) of vitamin C. Collagen molecules are synthetized and are then secreted into the extracellular space where they form fibrils that accumulate over the culture time period. In absence of vitamin C, a co-factor of the prolyl-4 hydroxylase, collagen molecules are not thermically stable preventing their assembly into fibrils in the extracellular space. This allows a better visualization of the newly-synthesized collagen molecules at the intracellular level. In presence of vitamin C, both intracellular and extracellular collagen immunoreactivity is observed. Intracellular immunoreactivity of collagen I, but not collagen V, was substantially decreased in shNrf2 fibroblasts (Figure 3b, quantification). Moreover, collagen I fibril staining in the ECM was less intense in shNrf2 fibroblasts compared to controls (Figure 3c), even though

quantification of the extracellular staining did not reveal statistical significance. (Figure 3b, quantification, p_value=0.06). Western blot analysis of total protein extracts of shNrf2 and shCtrl fibroblasts cultivated in presence of vitamin C, confirmed a significant decrease in collagen I amounts in shNrf2 extracts, whereas an increase in collagen V was observed but not statistically significant though not statistically significant (Figure 3c, quantification in supplementary Figure S6). Additionally, further Western blot analysis validated our transcriptomic data by revealing a significant decrease in the band density of fibrillin-2 in shNrf2 protein extracts compared to shCtrl, while a clear increase (n=3) in periostin expression level was observed in the three independent experiments, though not statistically significant (Figure 3c and supplementary Figure S6, quantification). We conclude that NRF2 shortage in HDF results in decreased collagen I synthesis and an imbalanced collagen I/V ratio that itself can explain the decrease of the collagen fibrils diameter.

NRF2 modulates ECM gene expression through a direct or indirect mechanism involving the transcription factor *ZNF469*

Putative antioxidant response element (ARE) binding peaks for NRF2 were found in the *COL1A1* and *COL1A2* proximal promoters using public NRF2 ChIP-seq data of human lung fibroblasts (IMR-90) (ENCODE Project Consortium, 2012; project GSE91565 in the NCBI-GEO database) (Figure 4a) indicating that NRF2 might directly regulate collagen I gene expression. We next explored the possibility of a transcriptional regulatory cascade. With this aim, we searched for potential ECM gene transcription regulators in the top 10 downregulated genes of our RNAseq data and identified *ZNF469* (Figure 4b). This was confirmed with RT-qPCR (Figure 4c). Additionally, we spotted an antioxidant response element (ARE) motif in the -1500/+100 bp promoter sequence of *ZNF469* at 1228 bp upstream of the transcription start site (TSS) (p-value=0.0000587), reinforcing our findings. Mutations in *ZNF469* are one of the

main molecular causes of Brittle Cornea Syndrome (BCS), a connective disease that affects corneal structure (Abu et al., 2008). ZNF469 is believed to be a transcription factor or an extra-nuclear regulator of fibrillar collagen genes, through a yet unknown pathway (Burkitt Wright et al., 2011; Rohrbach et al., 2013).

We next silenced *KEAP1* to investigate whether *ZNF469* is a basal or a stress-induced target of the KEAP1-NRF2 pathway. Silencing *KEAP1* provokes the elevation of NRF2 protein that in turn activates stress-induced targets but not basal targets (Malhotra et al., 2010). As expected, *NQO1* and *SLC7A11* were significantly upregulated in siKeap1 fibroblasts, while the basal target *HMOX1* remained unchanged (Figure 4d). *ZNF469* expression was not upregulated in siKeap1 fibroblasts indicating that *ZNF469* is a basal target of NRF2 (Figure 4d). We conclude that NRF2-mediated ECM gene regulation results, at least in part, from a transcriptional cascade through the basal target *ZNF469* identified here; a mechanism that is, to our knowledge, previously unreported.

ZNF469 regulates expression of collagen I genes with relevance for Brittle Corneal Syndrome (BCS)

To investigate if the collagen I genes are downstream targets of ZNF469, we next silenced *ZNF469* expression in HDF. A significant decrease in *COL1A1* and *COL1A2* expression was observed in siZNF469 fibroblasts, whereas expression of *COL5A1* remained unchanged (Figure 5a). Moreover, a marked decrease in intracellular collagen I immunoreactivity was observed in siZNF469 fibroblasts (Figure 5b), implying that *ZNF469* transcriptionally controls collagen I expression in HDF. Reduced ZNF469 activity thus results in a change in collagen I/V ratio, consistent to what we found in shNrf2 fibroblasts (Figure 2).

To assess the possible pathophysiological significance of our data, we analyzed expression of collagen I and V genes in dermal fibroblasts of two BCS patients (P1 and P2) carrying mutations

in *ZNF469* that both result in a premature termination codon (PTC) (Figure 5c) (Dhooge et al, 2021). No change in *ZNF469* expression level was observed in BCS fibroblasts (Figure 5d) indicating that these PTC-containing mRNAs escape non-sense-mediated RNA decay. In accordance with siZNF469 data, *COL1A1* and *COL1A2* expression levels were significantly reduced in BCS fibroblasts, whereas *COL5A1* and *COL5A2* expression remained unchanged (Figure 5d). Western blot analysis of fibroblast protein extracts from BCS patients *versus* healthy donors with antibodies to collagen I or to collagen V confirmed that BCS fibroblasts produced less collagen I while collagen V amounts are unchanged (Figure 5e). This results in a statistically significant decrease in the collagen I/V ratio in BCS fibroblasts (Figure 5e, quantification). Intracellular staining of BCS fibroblasts and healthy fibroblasts did not reveal a significant reduction of collagen I expression (supplementary Figure S7). We decided to investigate the ECM organization with TEM. The ECM produced by BCS fibroblasts of patients P1 and P2 showed striking abnormalities compared to controls, including reduced collagen fibrils and abundant disorganized filamentous components (Figure 5f), reminiscent to the ECM produced by shNrf2 (Figure 2b). Overall, these results support the assumption that ZNF469 deficiency impacts fibril formation in dermal fibroblasts and suggest a functional link between NRF2 and ZNF469 with relevance in BCS pathogenesis.

DISCUSSION

Our work identified NRF2 as a potential positive regulator of human dermal ECM homeostasis. Yet, NRF2-mediated matrisome gene expression was variable between the two different siNrf2-silenced HDF. This could be explained, at least in part, by a kinetic effect in cell response, suggesting that transcriptional downregulation of matrisome genes is not an acute response to NRF2 silencing. All NRF2 conventional targets involved in the well-known antioxidant, detoxification and metabolic functions of NRF2, were similarly downregulated in both siNR2-silenced HDF (Hayes and Dinkova-Kostova, 2014; Dodson et al., 2019). These genes must respond quickly to internal and external assaults to ensure cell survival and therefore must be highly transcriptionally inducible. In contrast, NFR2 may fine-tune matrisome gene expression secondary to a stress response. In agreement with this assumption, the downregulation of *COL1A1* and *COL1A2* genes was confirmed by using stably silenced shNrf2 fibroblasts that were cultivated over a longer period. Importantly, this implies that even a gradual decrease of NRF2 activity over a longer period of time, as observed in several tissues with aging (Bruns et al., 2015; Zhang et al., 2015; Schmidlin et al., 2019), could ultimately impact ECM composition.

Changes in the matrisome expression profile were reported in mouse skin fibroblasts in which NRF2 is constitutively activated (Hiebert et al., 2018). Interestingly, based on our analysis of Hiebert and collaborators' transcriptome data, 25 dysregulated matrisome genes out of 37 were also identified in our transcriptomic data (supplementary Table S2, in bold). However, among them, only 9 genes (ELN, POSTN, TIMP3, ANGPTL2, ANGPTL4, CXCL3, IL15, GPC1 and CLEC2D) showed the expected opposite direction in expression (supplementary Table S2, underlined). This may not be surprising as our study differs from the previous study (Hiebert et al, 2018) in possibly important points: NRF2 knockdown in human dermal papillary fibroblasts versus NRF2 constitutive activation in mouse

fibroblasts and distinct downstream effects, the downregulation of ZNF469 - as discussed below - versus the upregulation of PAI-1/SERPINE1 and induction of senescence.

Our data further substantiated that NRF2 regulates the expression of collagen genes, *COL1A1*, *COL1A2*, *COL10A1, COL24A1* and glycoprotein genes, *ELN*, *FBN2* and *POSTN*. Additionally, in this study, change in expression levels have been validated at the protein level for selected key genes, thereby validating our transcriptomic data. *COL10A1* and *COL24A1* were the most dysregulated collagen genes even though their expression was not expected in HDF. *COL10A1,* a marker of hypertrophic chondrocytes (Lu et al., 2014; Chen et al., 2019) was already found to be expressed in dermal fibroblasts in our previous studies (Nauroy et al., 2017; Haydont et al., 2020) though its functional significance in dermal fibroblasts remains unknown. Altogether our data underscores the critical role for NRF2 in regulating matrisome expression and the need of a strict NRF2 balance for a healthy dermal ECM. Finally, as oxidative stress also regulates ECM gene expression (Avantaggiato et al., 2014; Spadoni et al., 2015), our data provide evidence that, in addition to stress-induced NRF2 targets, basal targets participate in the regulation of ECM gene expression.

Most importantly, we distinctively showed here that changes in ECM gene expression upon NRF2 silencing was accompanied by abnormal fibrillogenesis. Dermal collagen fibers result from the tightly regulated assembly of three fibrillar collagens, types I, III and V, and other ECM fibril-forming regulators that together orchestrate fibrillogenesis (Shin et al., 2019). Collagen V is the initiator of collagen I fibrillogenesis and acts as a negative regulator of fibril diameters (Chanut-Delalande et al., 2004; Wenstrup et al., 2004; Sun et al., 2011). Strikingly, our data revealed that NRF2 shortage led to an unbalanced collagen I/V ratio that can explain both, the presence of abnormal thin collagen fibrils and their scarcity in shNrf2 ECM, which we observed with various microscopy techniques.

Fibrillogenesis is controlled by a number of additional ECM proteins (Bella and Hulmes, 2017). Some of them could also contribute to the shNrf2 ECM phenotype: *COL24A1* that is a negative regulator of collagen fibrils in corneal stroma (Koch et al., 2003) and *POSTN,* the role of which in fibrillogenesis is controversial. Thinner collagen fibrils were observed in *Postn*$^{-/-}$ mice, whereas human skin fibroblasts silenced for *POSTN* synthesized larger fibrils (Egbert et al., 2014; Norris et al., 2007). In our data *POSTN* was upregulated at the transcript and protein levels suggesting that *POSTN* serves as a negative regulator of collagen fibrillogenesis.

There is growing evidence for a role of NRF2 in ECM gene regulation (our data; Hiebert, 2021), but the underlying mechanisms remain elusive. NRF2 ChIP-seq and microarray analyses of *Nrf2*$^{-/-}$ mouse embryonic fibroblasts have identified *COL1A2* as a basal target of NRF2 (Malhotra et al., 2010). Accordingly, our *in silico* analysis identified putative antioxidant response element (ARE) binding motives for NRF2 in *COL1A1* and *COL1A2* proximal promoters. Moreover, our data suggested an indirect mechanism involving *ZNF469*, a novel NRF2 target identified in this study. ZNF469 was thought to act as a regulator of collagen expression and fibrillogenesis in BCS patients, a disorder that affects corneal stroma thickness and stiffness (Abu et al., 2008; Burkitt Wright, 2011; Rohrbach et al., 2013). Strikingly, collagen I expression was similarly affected in shNrf2, siZNF469 and BCS dermal fibroblasts. ZNF469 could be thus involved in the NRF2 transcription regulatory cascade controlling matrisome expression and ultimately ECM organization. The observed kinetic effect in the NRF2-mediated matrisome regulation in HDF reinforces the assumption of an indirect mechanism involving ZNF469.

In conclusion, we showed that reduced activity of NRF2 had direct and indirect functional consequences on the structure of the ECM network. Collagen I downregulation and abnormal collagen fibrils are the major modifications found in aged skin (Baumann, 2007; Shin et al., 2019) and in connective tissue diseases (Salamito et al., 2021). As a decrease in NRF2 signaling

contributes to the aging process (Heibert, 2021), NRF2 could represent an interesting target to improve skin aging signs. Along this line, $Sod3^{+/+}$ mice exhibited increased skin thickness and collagen production with aging at least in part by activating the Nrf2/HO-1 pathways (Lee et al. 2021). Moreover, our findings shed light on BCS pathogenesis and unveiled potential treatment targets for BCS.

MATERIAL AND METHODS

Dermal fibroblast isolation and culture

Human dermal papillary fibroblasts (HDF) were obtained from skin biopsies of three healthy Caucasian female donors aged from 22 to 31 years old (mammoplasty surgery) purchased from Icelltis (Toulouse, France), Alphenyx (Marseille, France) and Biopredic (Saint-Grégoire, France). Isolation and culture conditions of Brittle Cornea Syndrome (BCS) and healthy dermal fibroblasts are described in Supplementary Materials and Methods. Cells were cultivated in absence of vitamin C unless specified.

Transfection with siRNA

HDF were resuspended in culture media with 2% FBS, while transfection complexes were generated by mixing HiPerfect transfection reagent (Qiagen, Germany) and Stealth RNAi siRNAs (Thermo Fisher Scientific, France) (sequences in supplementary Table S3a) diluted in 2% FBS culture media, according to the manufacturer's instructions. Transfection complexes and cells were then seeded at a cell density of 5600 cell/cm2 and incubated for 72h at 37°C with 5% CO_2.

Redox status analysis

Redox status of the transfected cells was analyzed as described in Supplementary Materials and Methods.

Lentiviral-based shRNA transduction

MISSION® shRNA plasmids targeting NRF2 (shNrf2) and shRNA control (shCtrl) (SHC016) in pLKO.1-U6-shRNA-CMV-TAGRFP were purchased from Sigma-Aldrich (USA). shRNA sequences are listed in supplementary Table S3b. HDF transduction is described in Supplementary Material and Methods.

RT-qPCR analysis

Total RNA was extracted after 72h for siRNA HDF and at 80% confluency for the shRNA HDF and BCS fibroblasts samples and the corresponding controls. RNA extraction, cDNA synthesis, reverse transcription and qPCR were performed as described in Supplementary Materials and Methods. The supplementary Table S4 shows the list of primers used in the study.

RNA sequencing and data analysis

RNA sequencing experiments were performed using an Illumina NextSeq 500 sequencing platform in single end (75 bp). RNA samples were prepared as described above considering three biological replicates (3 donors) by condition (NT, siCtrl, siNrf2_1 and siNrf2_2). Concentration and quality of the RNA samples and data analysis are detailed in Supplementary Material and Methods.

Western blotting

Total proteins were extracted from cultured dermal fibroblasts (NRF2-silenced and shCrtl fibroblasts and BCS and healthy fibroblasts) and processed for Western blotting and densitometric quantification as described in Supplementary Materials and Methods.

Immunofluorescence staining and quantification

Human skin papillary fibroblasts were cultivated on glass cover slips during 5 to 8 days, in culture media with or without 1 mM vitamin C (Sigma-Aldrich, USA) for extracellular or extracellular staining, respectively. BCS fibroblasts and controls were seeded at 15,000 cells/well and grown for 48 hours in glass 8-chamber slides (Lab-Tek, Thermo Fisher Scientific, France) with 50 μg/ml of vitamin C (Sigma-Aldrich, USA). Immunostaining conditions and quantification of intracellular collagen I immunofluorescence are detailed in Supplementary Materials and Methods. Images were captured with a confocal Leica SP8 microscope (Leica, Germany) or an Axio Observer.Z1 fluorescence microscope (Zeiss, Germany).

SHG microscopy

Transduced fibroblasts (shCtrl and shNrf2) were cultivated for 8 days in culture media with 1 mM Vitamin C (Sigma-Aldrich, US) in 60 mm Petri dishes. Cultures were observed on a multiphoton microscope Leica SP8 coupled to a Spectra Physics Insight femto second laser, with an HC APO L 10x/0.3W objective (Leica, Germany). SHG signal emitted from the collagen fibers was epi-detected by illuminating the samples with a laser at 760 nm and collecting the signal with a non-descanned detector equipped with a 380/14 nm filter. Images were extracted using Image J software.

TEM analysis

Cells were cultivated for 8 days in culture media with 1 mM Vitamin C (Sigma-Alrich, US) in 35 mm Petri dishes. Cells were processed as described in Supplementary Materials and Methods. Ultra-thin sections were observed with MET JEOL 1400 Flash, equipped with a Gatan Rio 16 camera (Centre Technologique des Microstructures, LyMiC, Université Lyon1, France). Measurement of collagen fibrils diameter was performed using Fiji software.

AFM analysis

For AFM experiments, shCtrl and shNrf2 samples were decellularized as described in Supplementary Materials and Methods. AFM experiments were carried out with a Bioscope Resolve (Bruker Nano Surface) mounted on a fluorescent microscope (DMi8, Leica, Germany). Elastic modulus measurements were acquired using the PeakForce QNM (Quantitative Nanomechanical Mapping) AFM mode as described in Supplementary Materials and Methods. Each AFM measurement consisted in the analysis of force curves (FC) extracted from 50 µm × 50 µm areas. Each FC corresponds to 10,000 measurements from which the elastic modulus was derived by using the Hertz–Sneddon model (Sneddon, 1965). Aberrant values were eliminated for significant statistical analyses.

***In silico* analysis**

Identification of *NFE2L2* motifs in DNA promoter sequences and Public ChIP-seq data are described in Supplementary Materials and Methods.

Statistical analysis

Results are given as the mean ± SEM. Statistics were performed using GraphPad Prism 6 (La Jolla, California, USA). Comparison of RT-qPCR or protein expression used either ordinary one-way ANOVA or Student t-test according to the number of conditions to compare. ANOVA

for repeated measures and paired t-test were used when appropriate. Statistical analysis used for each experiment is indicated in the legend of the figure.

Data Availability Statement

Datasets related to this article can be found at https://www.ncbi.nlm.nih.gov/geo/query/acc.cgi?acc=GSE185129, hosted at NCBI-Gene Expression Omnibus (GEO) database.

ORCiD NUMBERS

Mélanie Salamito: https://orcid.org/0000-0002-0024-3323; Benjamin Gillet: https://orcid.org/0000-0002-6610-4537; Delfien Syx: https://orcid.org/0000-0001-9421-4496; Elisabeth Vaganay: https://orcid.org/0000-0002-6733-3067; Marilyne Malbouyres: https://orcid.org/0000-0002-0884-1387; Catherine Cerutti: https://orcid.org/0000-0002-7396-9387; Nicolas Tissot: https://orcid.org/0000-0002-9965-8640; Chloé Exbrayat-Héritier: https://orcid.org/0000-0002-3209-8298; Philippe Perez: https://orcid.org/0000-0001-7984-7164; Christophe Jones: https://orcid.org/0000-0002-7113-1847; Sandrine Hughes: https://orcid.org/0000-0003-3932-9180; Fransiska Malfait: https://orcid.org/0000-0002-5010-0304; Valérie Haydont: https://orcid.org/0000-0001-5126-2156; Sibylle Jäger: https://orcid.org/0000-0001-8102-7149; Florence Ruggiero: https://orcid.org/0000-0003-2915-5359

AUTHOR CONTRIBUTION

Conceptualization: SJ, FR; Data curation: SH; Formal analysis: MS, DS, SH, CC, CEH, VH; Funding acquisition: FR; Investigation: MS, BG, DS, EV, MM, CC, NT, CEH; Methodology: BG, EV, NT; Resources: MS, PP, CJ; FM; Project administration: SJ, FR; Supervision: FM, VH, SJ, FR; Validation: MS, CC; Visualization: MS; Writing - review/editing: DS, VH, SH; Writing - original draft preparation: MS, SJ, FR

CONFLICT OF INTEREST

MS, NT, PP, CJ, VH and SJ are employees of L'Oréal Research and Innovation. FR declares the receipt of a grant from L'Oréal Research and Innovation. BG, DS, EV, MM, CC, CEH, SH and FM state no conflict of interest.

ACKNOWLEDGEMENTS

We thank Y. Ben Khalifa, J-M Vanacker, L. Marrot and L. Breton for sharing their great expertise and Z. Malfait for excellent technical assistance. We acknowledge the contribution of SFR Biosciences (UAR3444/CNRS, US8/Inserm, ENS de Lyon, UCBL) facilities for the lentivectors production, B. Blanquier for helpful advices in RT-qPCR data analysis and the "Centre Technologique des Microstructures" (LyMiC, University Lyon1, France). DS and FM are a senior postdoctoral researcher and a senior clinical researcher, respectively, supported by the Research Foundation Flanders (FWO), Belgium.

REFERENCES

Abu A, Frydman M, Marek D, Pras E, Nir U, Reznik-Wolf H, et al. Deleterious mutations in the Zinc-Finger 469 gene cause brittle cornea syndrome. Am J Hum Genet 2008; 82:1217–1222. https://doi.org/10.1016/j.ajhg.2008.04.001

Ambrozova N, Ulrichova J, Galandakova A. Models for the study of skin wound healing. The role of Nrf2 and NF-κB. Biomed Pap Med Fac Univ Palacky Olomouc Czech Repub 2017;161:1–13. https://doi.org/10.5507/bp.2016.063

Anders S, Huber W. Differential expression analysis for sequence count data. Genome Biol 2010;11:R106. https://doi.org/10.1186/gb-2010-11-10-r106

Ashworth JL, Murphy G, Rock MJ, Sherratt MJ, Shapiro SD, Shuttleworth CA, et al. Fibrillin degradation by matrix metalloproteinases: implications for connective tissue remodelling. Biochem J 1999;340:171-181

Avantaggiato A, Palmieri A, Bertuzzi G, Carinci F. Fibroblasts behavior after N-acetylcysteine and amino acids exposure: extracellular matrix gene expression. Rejuvenation Res 2014;17:285–290. https://doi.org/10.1089/rej.2013.1511

Bancelin S, Aimé C, Coradin T, Schanne-Klein M-C. In situ three-dimensional monitoring of collagen fibrillogenesis using SHG microscopy. Biomed Opt Express 2012;3:1446–1454. https://doi.org/10.1364/BOE.3.001446

Bancelin S, Lynch B, Bonod-Bidaud C, Ducourthial G, Psilodimitrakopoulos S, Dokládal P, et al. Ex vivo multiscale quantitation of skin biomechanics in wild-type and genetically-modified mice using multiphoton microscopy. Sci Rep 2015;5-17635. https://doi.org/10.1038/srep17635

Baumann L. Skin ageing and its treatment. J Pathol 2012;211:241–251. https://doi.org/10.1002/path.2098

Bella J, Hulmes DJS. Fibrillar Collagens. Subcell Biochem 2017;82:457–490. https://doi.org/10.1007/978-3-319-49674-0_14

Bonod-Bidaud C, Beraud M, Vaganay E, Delacoux F, Font B, Hulmes DJS, et al. Enzymatic cleavage specificity of the proα1(V) chain processing analyzed by site-directed mutagenesis. Biochem J 2007;405:299-306. https://doi.org/10.1042/bj20070051

Bonod-Bidaud C, Roulet M, Hansen U, Elsheikh A, Malbouyres M, Ricard-Blum S, et al. In vivo evidence for a bridging role of a collagen V subtype at the epidermis-dermis interface. J Invest Dermatol 2012;132:1841-1849. https://doi.org/10.1038/jid.2012.56

Brück J, Dringen R, Amasuno A, Pau-Charles I, Ghoreschi K. A review of the mechanisms of action of dimethylfumarate in the treatment of psoriasis. Exp Dermatol 2018;27:611–624. https://doi.org/10.1111/exd.13548

Bruns DR, Drake JC, Biela LM, Peelor FF, Miller BF, Hamilton KL. Nrf2 Signaling and the Slowed Aging Phenotype: Evidence from Long-Lived Models. Oxid Med Cell Longev 2015;732596. https://doi.org/10.1155/2015/732596

Burkitt Wright EMM, Spencer HL, Daly SB, Manson FDC, Zeef LAH, Urquhart J, et al. Mutations in PRDM5 in brittle cornea syndrome identify a pathway regulating extracellular matrix development and maintenance. Am J Hum Genet 2011;88:767-777. doi.org/10.1016/j.ajhg.2011.05.007

Chanut-Delalande H, Bonod-Bidaud C, Cogne S, Malbouyres M, Ramirez F, Fichard A, et al. Development of a functional skin matrix requires deposition of collagen V heterotrimers. Mol Cell Biol 2004;24:6049-6057. https://doi.org/10.1128/MCB.24.13.6049-6057.2004

Chen J, Chen F, Bian H, Wang Q, Zhang X, Sun L, et al. Hypertrophic chondrocyte-specific Col10a1 controlling elements in Cre recombinase transgenic studies. Am J Transl Res 2019;11:6672-6679.

Dhooge T, Van Damme T, Syx D, Mosquera LM, Nampoothiri S, Radhakrishnan A, et al. More than meets the eye: Expanding and reviewing the clinical and mutational spectrum of brittle cornea syndrome. Hum Mutat 2021;42:711-730. https://doi.org/10.1002/humu.24199

Dobin A, Davis CA, Schlesinger F, Drenkow J, Zaleski C, Jha S, et al. STAR: ultrafast universal RNA-seq aligner. Bioinformatics 2013;29:15-21. https://doi.org/10.1093/bioinformatics/bts635

Dodson M, de la Vega MR, Cholanians AB, Schmidlin CJ, Chapman E, Zhang DD. Modulating NRF2 in Disease: Timing Is Everything. Annu Rev Pharmacol Toxicol 2019;59: 555-575. https://doi.org/10.1146/annurev-pharmtox-010818-021856

Egbert M, Ruetze M, Sattler M, Wenck H, Gallinat S, Lucius R, et al. The matricellular protein periostin contributes to proper collagen function and is downregulated during skin aging. J Dermatol Sci 2014;73:40-48. https://doi.org/10.1016/j.jdermsci.2013.08.010

ENCODE Project Consortium. An integrated encyclopedia of DNA elements in the human genome. Nature 2012;489:57-74. https://doi.org/10.1038/nature11247

Ewald CY, Landis JN, Porter Abate J, Murphy CT, Blackwell TK. Dauer-independent insulin/IGF-1-signalling implicates collagen remodelling in longevity. Nature 2015;519: 97-101. https://doi.org/10.1038/nature14021

Frantz C, Stewart KM, Weaver VM. The extracellular matrix at a glance. J Cell Sci 2010;123: 4195-4200. https://doi.org/10.1242/jcs.023820

Gęgotek A, Skrzydlewska E. The role of transcription factor Nrf2 in skin cells metabolism. Arch Dermatol Res 2015;307:385-396. https://doi.org/10.1007/s00403-015-1554-2

Haydont V, Bernard BA, Fortunel NO. Age-related evolutions of the dermis: Clinical signs, fibroblast and extracellular matrix dynamics. Mech Ageing Dev 2019a;177:150-156. https://doi.org/10.1016/j.mad.2018.03.006

Haydont V, Neiveyans V, Fortunel NO, Asselineau D. Transcriptome profiling of human papillary and reticular fibroblasts from adult interfollicular dermis pinpoints the “tissue skeleton” gene network as a component of skin chrono-ageing. Mech Ageing Dev 2019b,179:60-77. https://doi.org/10.1016/j.mad.2019.01.003

Haydont V, Neiveyans V, Perez P, Busson É, Lataillade J, Asselineau D et al. Fibroblasts from the Human Skin Dermo-Hypodermal Junction are Distinct from Dermal Papillary and Reticular Fibroblasts and from Mesenchymal Stem Cells and Exhibit a Specific Molecular Profile Related to Extracellular Matrix Organization and Modeling. Cells 2020;9. https://doi.org/10.3390/cells9020368

Hayes JD, Dinkova-Kostova AT. The Nrf2 regulatory network provides an interface between redox and intermediary metabolism. Trends Biochem Sci 2014;39:199-218. https://doi.org/10.1016/j.tibs.2014.02.002

Hiebert P. The Nrf2 transcription factor: A multifaceted regulator of the extracellular matrix. Matrix Biol Plus 2021;10:100057. https://doi.org/10.1016/j.mbplus.2021.100057

Hiebert P, Werner S. Regulation of Wound Healing by the NRF2 Transcription Factor-More Than Cytoprotection. Int J Mol Sci 2019;20. https://doi.org/10.3390/ijms20163856

Hiebert P, Wietecha MS, Cangkrama M, Haertel E, Mavrogonatou E, Stumpe M, et al. Nrf2-Mediated Fibroblast Reprogramming Drives Cellular Senescence by Targeting the Matrisome. Dev Cell 2018;46:145-161.e10. https://doi.org/10.1016/j.devcel.2018.06.012

Huang Y, Li W, Su Z, Kong A-NT. The complexity of the Nrf2 pathway: beyond the antioxidant response. J Nutr Biochem 2015;26:1401-1413. https://doi.org/10.1016/j.jnutbio.2015.08.001

Kavian N, Mehlal S, Jeljeli M, Saidu NEB, Nicco C, Cerles O, et al. The Nrf2-Antioxidant Response Element Signaling Pathway Controls Fibrosis and Autoimmunity in Scleroderma. Front Immunol 2018;9:1896. https://doi.org/10.3389/fimmu.2018.01896

Kobayashi EH, Suzuki T, Funayama R, Nagashima T, Hayashi M, Sekine H, et al. Nrf2 suppresses macrophage inflammatory response by blocking proinflammatory cytokine transcription. Nat Commun 2016;7:11624. https://doi.org/10.1038/ncomms11624

Koch M, Laub F, Zhou P, Hahn RA, Tanaka S, Burgeson RE, et al. Collagen XXIV, a vertebrate fibrillar collagen with structural features of invertebrate collagens: selective expression in developing cornea and bone. J Biol Chem 203;278:43236-43244. https://doi.org/10.1074/jbc.M302112200

Lee MJ, Agrahari G, Kim H-Y, An E-J, Chun K-H, Kang H et al. Extracellular Superoxide Dismutase Prevents Skin Aging by Promoting Collagen Production through the Activation of AMPK and Nrf2/HO-1 Cascades. J Invest Dermatol 2021;141:2344-2353.e7. https://doi.org/ 10.1016/j.jid.2021.02.757

Lu Y, Qiao L, Lei G, Mira RR, Gu J, Zheng Q. Col10a1 gene expression and chondrocyte hypertrophy during skeletal development and disease. Frontiers in Biology 2014;9:195-204. https://doi.org/10.1007/s11515-014-1310-6

Malhotra D, Portales-Casamar E, Singh A, Srivastava S, Arenillas D, Happel C, et al. Global mapping of binding sites for Nrf2 identifies novel targets in cell survival response through ChIP-Seq profiling and network analysis. Nucleic Acids Res 2010;38: 5718-5734. https://doi.org/10.1093/nar/gkq212

Marrot L. Pollution and Sun Exposure: A Deleterious Synergy. Mechanisms and Opportunities for Skin Protection. Curr Med Chem 2018;25:5469-5486. https://doi.org/10.2174/0929867324666170918123907

Murphy-Marshman H, Quensel K, Shi-Wen X, Barnfield R, Kelly J, Peidl A, et al. Antioxidants and NOX1/NOX4 inhibition blocks TGFβ1-induced CCN2 and α-SMA expression in dermal and gingival fibroblasts. PLoS ONE 2017;12:e0186740. https://doi.org/10.1371/journal.pone.0186740

Naba A, Clauser KR, Hoersch S, Liu H, Carr SA, Hynes RO. The matrisome: in silico definition and in vivo characterization by proteomics of normal and tumor extracellular matrices. Mol Cell Proteomics 2012;11:M111.014647. https://doi.org/10.1074/mcp.M111.014647

Nauroy P, Barruche V, Marchand L, Nindorera-Badara S, Bordes S, Closs B, et al. Human Dermal Fibroblast Subpopulations Display Distinct Gene Signatures Related to Cell Behaviors and Matrisome. J Invest Dermatol 2017;137:1787-1789. https://doi.org/10.1016/j.jid.2017.03.028

Norris RA, Damon B, Mironov V, Kasyanov V, Ramamurthi A, Moreno-Rodriguez R, et al. Periostin regulates collagen fibrillogenesis and the biomechanical properties of connective tissues. J Cell Biochem 2007;101:695-711. https://doi.org/10.1002/jcb.21224

Nyström A, Bruckner-Tuderman L. Matrix molecules and skin biology. Semin Cell Dev Biol 2019;89:136-146. https://doi.org/10.1016/j.semcdb.2018.07.025

Ricard-Blum S, Ruggiero F. The collagen superfamily: from the extracellular matrix to the cell membrane. Pathol Biol 2005;53:430–442. https://doi.org/10.1016/j.patbio.2004.12.024

Rohrbach M, Spencer HL, Porter LF, Burkitt-Wright EMM, Bürer C, Janecke A, et al. ZNF469 frequently mutated in the brittle cornea syndrome (BCS) is a single exon gene possibly regulating the expression of several extracellular matrix components. Mol Genet. Metab 2013;109:289-295. https://doi.org/10.1016/j.ymgme.2013.04.014

Salamito M, Nauroy P, Ruggiero F. The Collagen Superfamily: Everything You Always Wanted to Know, in: Ruggiero, F. (Ed.), The Collagen Superfamily and Collagenopathies, Biology of Extracellular Matrix. Springer International Publishing, Cham, 2021;1-22. https://doi.org/10.1007/978-3-030-67592-9_1

Schäfer M, Dütsch S, auf dem Keller U, Werner S. Nrf2: a central regulator of UV protection in the epidermis. Cell Cycle 2010;9:2917–2918. https://doi.org/10.4161/cc.9.15.12701

Schmidlin CJ, Dodson MB, Madhavan L, Zhang DD. Redox regulation by NRF2 in aging and disease. Free Radic Biol Med 2019;134:702-707. https://doi.org/10.1016/j.freeradbiomed.2019.01.016

Shin J-W, Kwon S-H, Choi J-Y, Na J-I, Huh C-H, Choi H-R, et al. Molecular Mechanisms of Dermal Aging and Antiaging Approaches. Int J Mol Sci 2019;20. https://doi.org/10.3390/ijms20092126

Sneddon IN. The relation between load and penetration in the axisymmetric boussinesq problem for a punch of arbitrary profile. Inter J Eng Sci 1965;3:47-57. https://doi.org/10.1016/0020-7225(65)90019-4

Spadoni T, Svegliati Baroni S, Amico D, Albani L, Moroncini G, Avvedimento EV, et al. A reactive oxygen species-mediated loop maintains increased expression of NADPH oxidases 2 and 4 in skin fibroblasts from patients with systemic sclerosis. Arthritis Rheumatol 2015;67:1611-1622. https://doi.org/10.1002/art.39084

Sparavigna A. Role of the extracellular matrix in skin aging and dedicated treatment - State of the art. Plast Aesthet Res 2020;7-14. https://doi.org/10.20517/2347-9264.2019.73

Statzer C, Jongsma E, Liu SX, Dakhovnik A, Wandrey F, Mozharovskyi P, et al. Youthful and age-related matreotypes predict drugs promoting longevity. Aging Cell 2021;20: e13441. https://doi.org/10.1111/acel.13441

St-Pierre J, Drori S, Uldry M, Silvaggi JM, Rhee J, Jäger S, et al. Suppression of reactive oxygen species and neurodegeneration by the PGC-1 transcriptional coactivators. Cell 2006;127:397-408. https://doi.org/10.1016/j.cell.2006.09.024

Sun M, Chen S, Adams SM, Florer JB, Liu H, Kao WW-Y, et al. Collagen V is a dominant regulator of collagen fibrillogenesis: dysfunctional regulation of structure and function in a corneal-stroma-specific Col5a1-null mouse model. J. Cell. Sci. 2011;124: 4096-4105. https://doi.org/10.1242/jcs.091363

Suzuki T, Muramatsu A, Saito R, Iso T, Shibata T, Kuwata K, et al. Molecular Mechanism of Cellular Oxidative Stress Sensing by Keap1. Cell Rep 2019;28:746-758.e4. https://doi.org/10.1016/j.celrep.2019.06.047

Taha IN, Naba A. Exploring the extracellular matrix in health and disease using proteomics. Essays Biochem 2019;63:417-432. https://doi.org/10.1042/EBC20190001

Theocharis AD, Manou D, Karamanos NK. The extracellular matrix as a multitasking player in disease. FEBS J 2019;286:2830-2869. https://doi.org/10.1111/febs.14818

Tonelli C, Chio IIC, Tuveson DA. Transcriptional Regulation by Nrf2. Antioxid Redox Signal 2018;29:1727-1745. https://doi.org/10.1089/ars.2017.7342

Wenstrup RJ, Florer JB, Brunskill EW, Bell SM, Chervoneva I, Birk DE. Type V collagen controls the initiation of collagen fibril assembly. J Biol Chem 2004;279:53331-53337. https://doi.org/10.1074/jbc.M409622200

Wu R, Zhang H, Zhao M, Li J, Hu Y, Fu J, et al. Nrf2 in keratinocytes protects against skin fibrosis via regulating epidermal lesion and inflammatory response. Biochem Pharmacol 2020;174-113846. https://doi.org/10.1016/j.bcp.2020.113846

Zhang H, Davies KJA, Forman HJ. Oxidative stress response and Nrf2 signaling in aging. Free Radic Biol Med 2015;88:314-336. https://doi.org/10.1016/j.freeradbiomed.2015.05.036

FIGURE LEGENDS

Figure 1: Transcriptomic analysis of NRF2 silenced HDF. (**a**) Repartition of the differentially expressed genes in siNrf2_1 and siNrf2_2 conditions vs the siCtrl among the different gene categories and matrisome subsets (fold change set up at 2 and p-value ≤ 0.05). (**b**) Tissue skeleton analysis of the genes that are significant differentially expressed genes in siNrf2_1 and siNrf2_2 vs. siCtrl (fold change set up at 2 and p-value ≤ 0.05), according to the different tissue skeleton categories defined in (Haydont *et al*., 2019). (**c**) Core matrisome genes and (**d**) STRING analysis of matrisome genes commonly differentially expressed in both siNrf2 (fold change set up at 1.4 and p-value ≤0.05).

Figure 2: Stable silencing of NRF2 in fibroblasts affects collagen fibrils diameter. (**a**) Large acquisitions of collagen fibers produced by shCtrl and shNrf2 fibroblasts, after 8 days of culture with vitamin C detected by SHG microscopy. Scale bars = 1µm. (**b**) TEM acquisitions of the ECM produced by shCtrl and shNrf2 fibroblasts; right images, zoom of boxed areas. Arrows indicate collagen fibers; black (ShCtrl) and white (shNrf2) asterisks indicate filamentous ECM components. Arrowheads point to regularly spaced, electron dense proteoglycan-like aggregates that decorate collagen fibers. Scale bars = 200 nm. (**c**) Quantification of the collagen fibrils diameter from TEM acquisitions (b). Statistics were done using an unpaired t-test (n_fibrils = 148). Asterisks indicate p-value: ***≤ 0.001. Errors bars represent mean ± SEM. (**d**) Distribution of the collagen fibrils diameter from the TEM acquisitions (b) according to their diameter every 2 nm.

Figure 3: Collagen I to collagen V ratio is modified in NRF2 silenced fibroblasts. (**a**) RT-qPCR analysis of *COL1A1, COL1A2* and *COL5A1* in shCtrl and shNrf2 fibroblasts. Statistics

were done using a paired t-test (n_experiments = 6). Asterisks indicate p-value: * ≤ 0.05, ** ≤ 0.01, ns: non-significant. Errors bars represent mean ± SEM. (**b**) Left, Immunofluorescence staining of shCtrl and shNrf2 fibroblasts cultured for 8 days in absence (intracellular) or presence (intra+extracellular) of vitamin C. Images are representative of 3 independent experiments. Scale bars = 50µm. Right, Quantification (n=3). Statistics were done using a T-test unpaired and non-parametric (Mann-whitney). Errors bars represent mean ± SEM, **** p-value <0.0001, ns: non-significant. (**c**) Representative Western blot membrane of ECM proteins expression levels of shCtrl and shNrf2 fibroblast cell layers (n=3). Fibrillin-2 is detected as a ~200 kDa band and a ~45 kDa resulting a major proteolytic cleavage product as previously reported (Ashworth et al, 1999). Detection of GAPDH and TGX stain-free images are protein loading controls.

Figure 4: Direct and undirect mechanisms for NRF2 action on collagen I genes. (**a**) Potential binding sites of *NFE2L2* on *COL1A1* and *COL1A2* human genes: -1500/+100bp from the transcription start site (TSS) of *COL1A1* and *COL1A2* sequences were scanned for matches to human *NFE2L2* motif (ARE: MA0150.1, JASPAR database) (upper panel) using the MEME-FIMO on-line tool (bottom panel). The p-value of the motif occurrence is obtained after comparison with random sequences of the same length and it gives the probability of getting one motif match simply by chance. Motif occurrences with p-value <0.0002 were selected. (**b**) Heatmap of the 10 most significantly downregulated genes in siNrf2 fibroblasts compared to controls. Fold changes are represented on a red (0 fold) to light green (10 fold) scale. (**c**) RT-qPCR of *ZNF469* expression in shNRF2 fibroblasts. Statistics were done a paired t-test (n=3). Errors bars represent mean ± SEM; p-values: *≤0.05, **≤0.01. (**d**) RT-qPCR of NRF2 targets in siNrf2 and siKeap1 conditions. Statistics were done using the ordinary one-way ANOVA

test (n_donor=3, in duplicate). Errors bars represent mean ± SEM; p-value: ***≤0.001, **≤0.01, *≤0.05, ns: non-significant.

Figure 5: ZNF469 silenced and BCS fibroblasts display the same collagen gene expression pattern as NRF2 silenced fibroblasts. (**a**) RT-qPCR analysis of *ZNF469* and collagen genes expression and (**b**) collagen I immunofluorescence staining of siCtrl and siZNF469 fibroblasts. (**c**) Location of the *ZNF469* mutations identified in BCS patients (P1 and P2). Scale bars = 50µm. (**d**) RT-qPCR analysis of *ZNF469* and collagen genes. **(e)** Representative Western blot membrane of collagens I (ColIα1) and V (ColVα1) expression levels. GAPDH, protein loading control. Histogram shows densitometric quantification of the collagen I/V ratio. Samples were run on a same gel for each experiment. (**f**) TEM acquisitions of BCS (P1 and P2) and healthy (Ctrl) cultured fibroblasts. Arrows, collagen fibers; asterisks, filamentous ECM components. Scale bars = 2µm. (**a,d,e**) Statistics were done using the ordinary one-way ANOVA test (**a,b**) or Student's t-test (**e**). Errors bars represent mean ± SEM, n=3, p-value: *≤ 0.05, ***≤0.001, ns: non-significant.

Figure 1

a

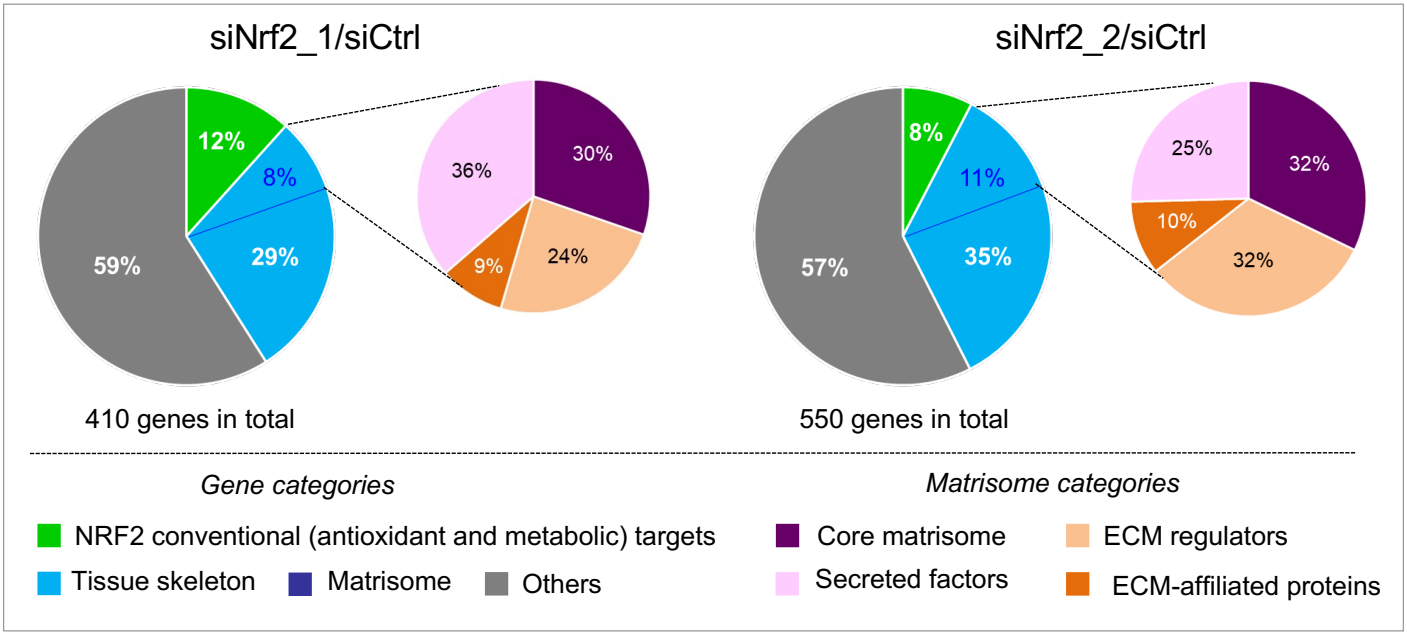

b

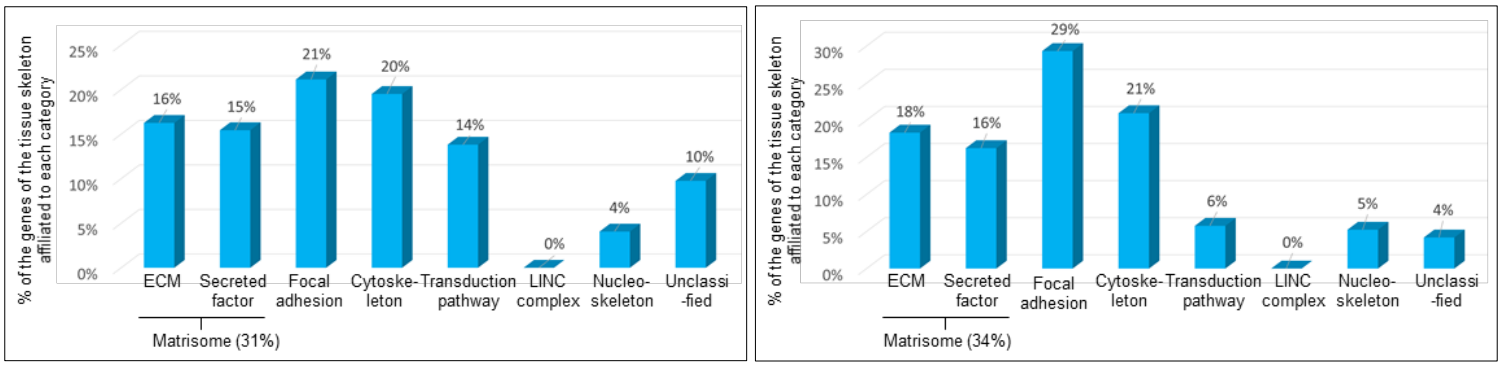

c

Core matrisome	Gene	Dysregulation in siNrf2_1 and 2 vs. siCtrl	
Collagens	*COL1A1*	DOWN	DOWN
	COL1A2	DOWN	DOWN
	COL10A1	UP	UP
	COL24A1	DOWN	DOWN
ECM Glycoproteins	*COMP*	UP	UP
	ELN	UP	UP
	FBN2	DOWN	DOWN
	FNDC1	DOWN	DOWN
	IGSF10	DOWN	DOWN
	NTN1	DOWN	DOWN
	POSTN	UP	UP
	SVEP1	DOWN	DOWN
Proteoglycans	*ESM1*	UP	UP

d

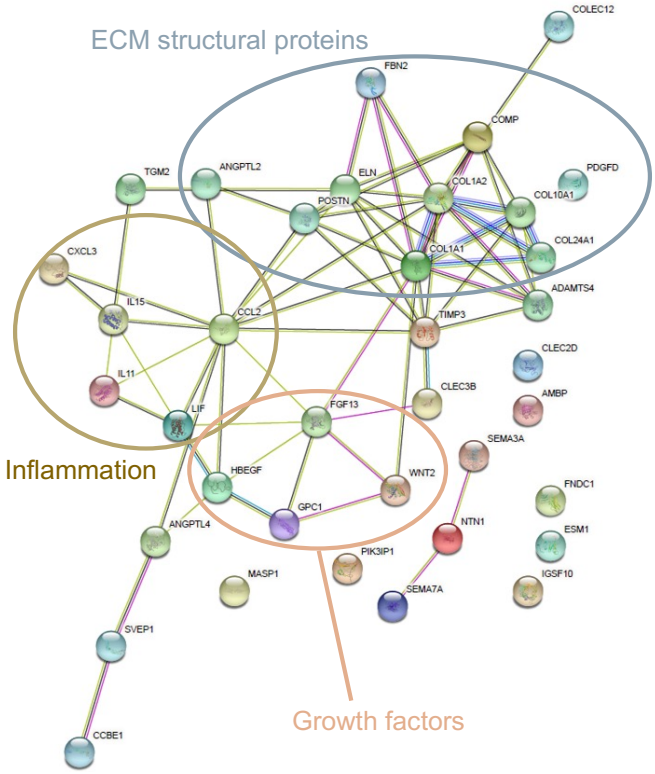

Figure 2

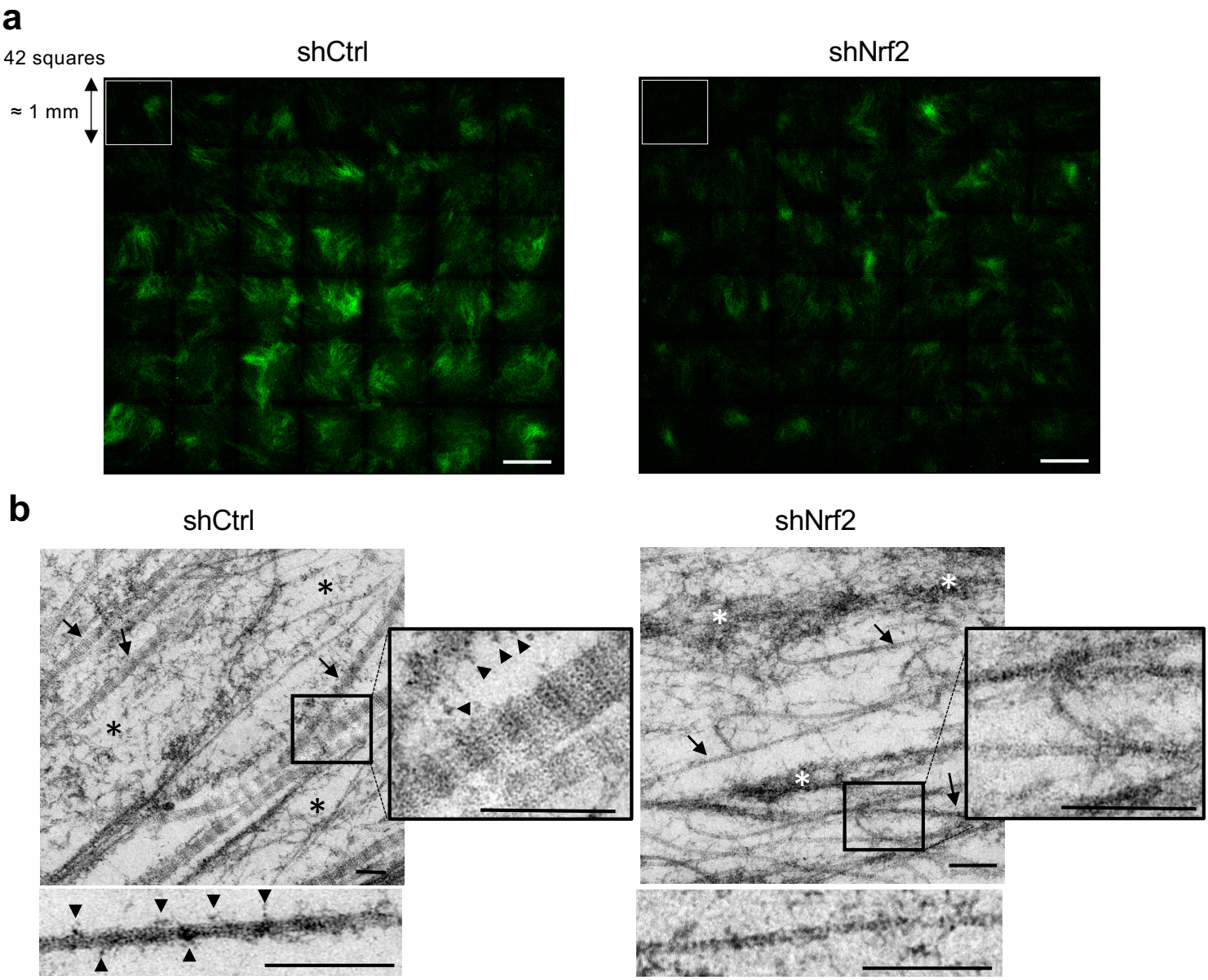
a
42 squares
≈ 1 mm
shCtrl
shNrf2
b
shCtrl
shNrf2
c
Mean of fibril diameter (nm) ± SEM
***
23.46 ± 0.61
17.50 ± 0.23
shCtrl
shNrf2
d
Frequency
shCtrl
shNrf2
Fibril diameter (nm)

Figure 4

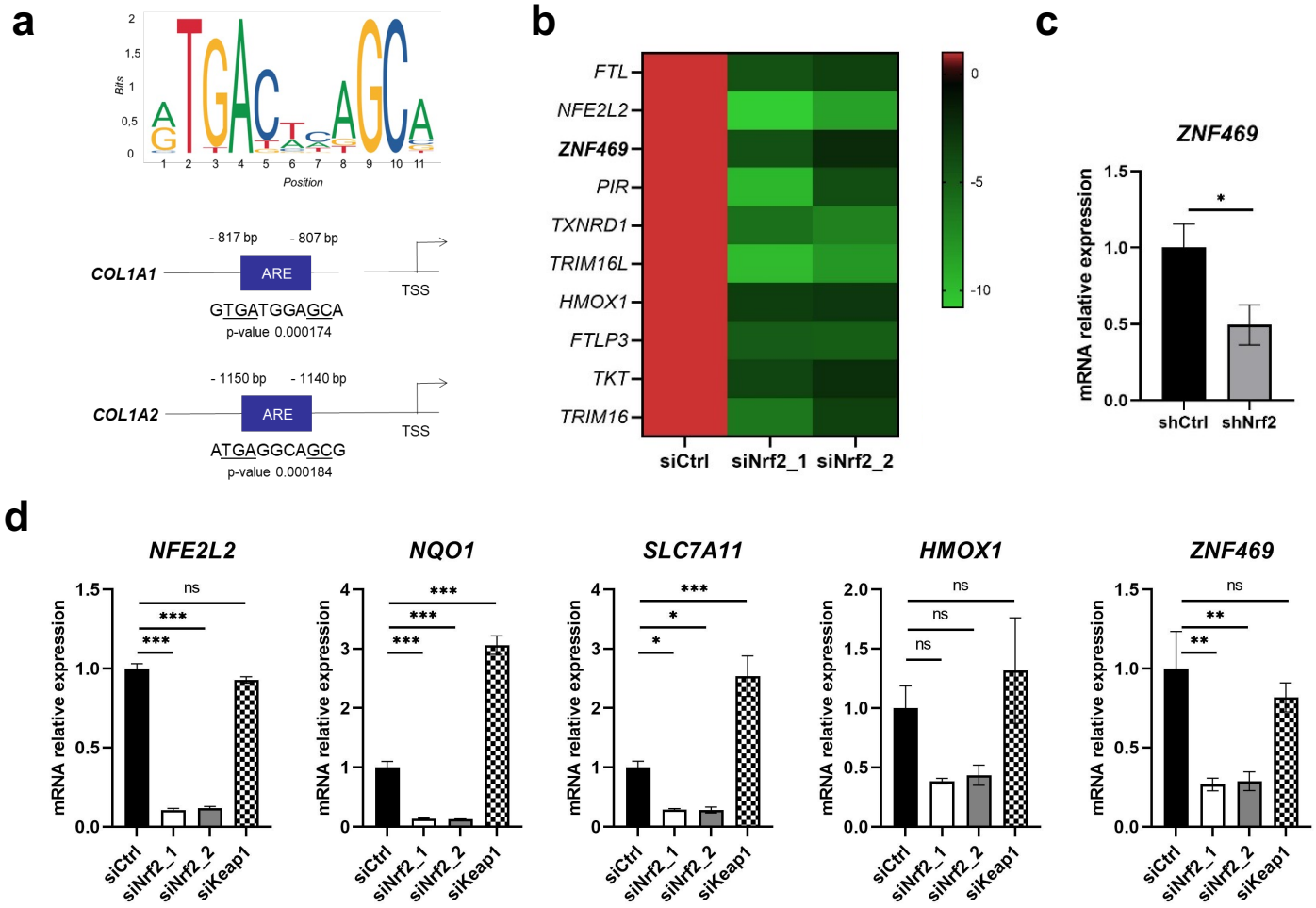
a
Bits
Position
- 817 bp
- 807 bp
COL1A1
ARE
TSS
GTGATGGAGCA
p-value 0.000174
- 1150 bp
- 1140 bp
COL1A2
ARE
TSS
ATGAGGCAGCG
p-value 0.000184
b
FTL
NFE2L2
ZNF469
PIR
TXNRD1
TRIM16L
HMOX1
FTLP3
TKT
TRIM16
siCtrl
siNrf2_1
siNrf2_2
c
ZNF469
mRNA relative expression
shCtrl
shNrf2
d
NFE2L2
NQO1
SLC7A11
HMOX1
ZNF469
mRNA relative expression
siCtrl
siNrf2_1
siNrf2_2
siKeap1

Figure 3

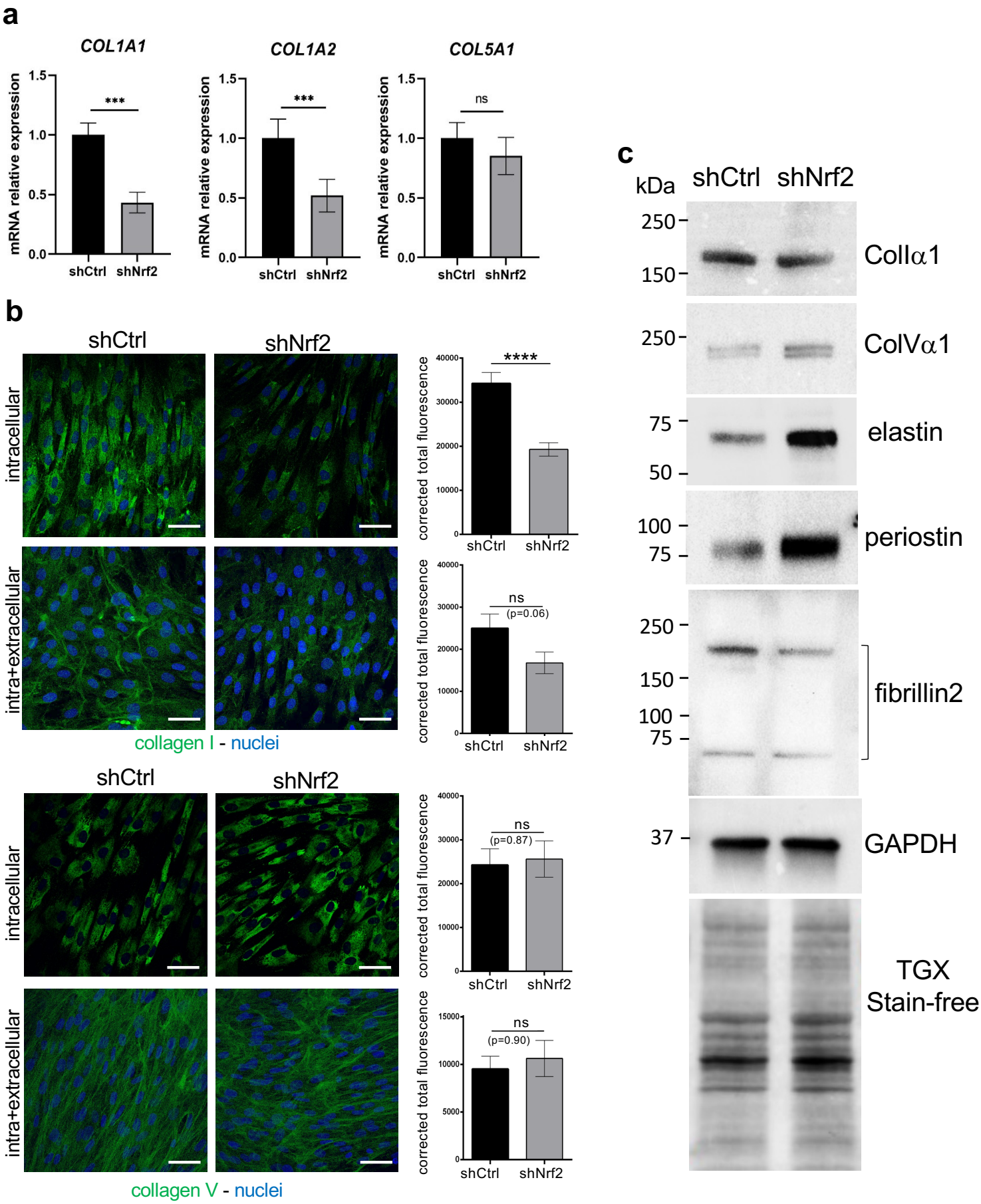
a
COL1A1
COL1A2
COL5A1
mRNA relative expression
1.5
1.0
0.5
0.0
***
ns
shCtrl
shNrf2
b
shCtrl
shNrf2
intracellular
intra+extracellular
collagen I - nuclei
collagen V - nuclei
corrected total fluorescence
40000
30000
20000
10000
0
****
ns
(p=0.06)
(p=0.87)
(p=0.90)
15000
5000
c
kDa
shCtrl
shNrf2
250
150
100
75
50
37
ColIα1
ColVα1
elastin
periostin
fibrillin2
GAPDH
TGX
Stain-free

Figure 5

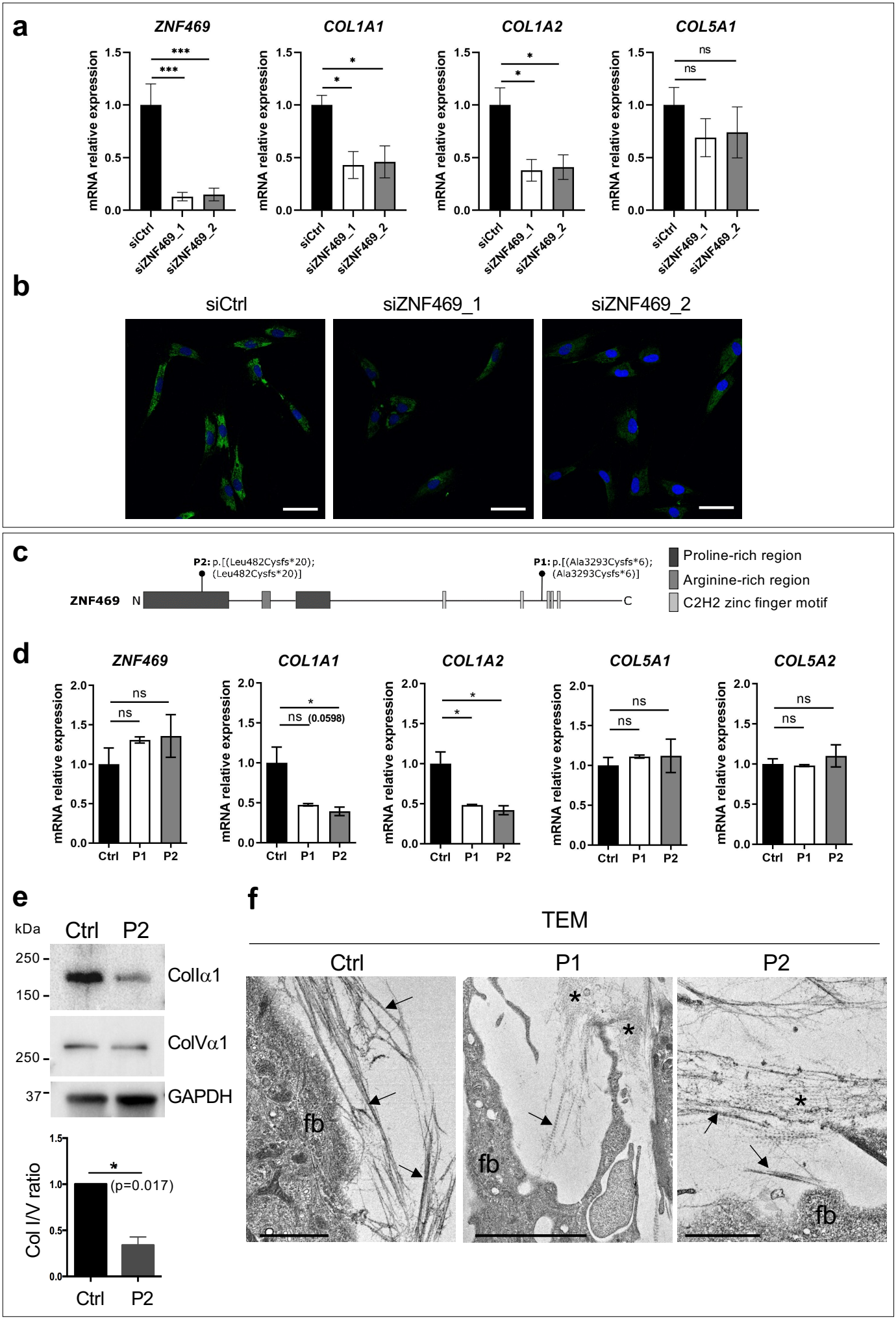
a
ZNF469
COL1A1
COL1A2
COL5A1
mRNA relative expression
siCtrl
siZNF469_1
siZNF469_2
b
siCtrl
siZNF469_1
siZNF469_2
c
P2: p.[(Leu482Cysfs*20);(Leu482Cysfs*20)]
P1: p.[(Ala3293Cysfs*6);(Ala3293Cysfs*6)]
ZNF469
N
C
Proline-rich region
Arginine-rich region
C2H2 zinc finger motif
d
ZNF469
COL1A1
COL1A2
COL5A1
COL5A2
mRNA relative expression
Ctrl
P1
P2
ns
(0.0598)
e
kDa
Ctrl
P2
250
150
ColIα1
250
ColVα1
37
GAPDH
Col I/V ratio
(p=0.017)
f
TEM
Ctrl
P1
P2
fb

SUPPLEMENTARY MATERIALS AND METHODS

Dermal fibroblast isolation and culture

Human skin samples were sliced according to depth using a dermatome to dissect the papillary dermis areas. A cut was performed at the depth of 300 µm, thus separating the upper part of the samples, which contained the epidermis and the papillary dermis. After removing the epidermis by treatment with 2.4 U/ml dispase (Roche, Boulogne-Billancourt, France) and then mechanical dissection, papillary fibroblasts were extracted by digestion of the tissue in type II collagenase 0.2% (Gibco, France). Human dermal papillary fibroblasts were stored in liquid nitrogen until used. For experiments, cells were cultured in Modified Eagle's Medium (MEM) (Gibco, France) supplemented with 10% of Fetal Bovine Serum (FBS) (HyClone, UK), non-essential amino acid solution (NEAA) (Gibco, France), 1 mM of sodium pyruvate (Gibco, France), 2 mM of glutamine (Gibco, France), 20 U/ml of penicillin/streptomycin (Merck Millipore, Germany) and antibiotic-antimycotic (Gibco, France) in a 90% humidified incubator at 37°C with 5% CO_2. Cells were seeded at 4000 cell/cm^2, unless stated differently, and cultivated until the end of passage 7 (P7).

Skin fibroblasts of Brittle Cornea Syndrome (BCS) patients with mutations in *ZNF469* (Dhooge et al, 2021) were used in this study. BCS and healthy volunteers were obtained from a punch biopsy (maximum 5 mm diameter) from the inner side of the upper arm. To obtain a primary dermal fibroblast culture, the biopsy was cut and individual skin pieces were seeded on the bottom of a T25 flask with 1.5 ml of supplemented DMEM medium. After 72h, the culture medium was gradually increased over two weeks to 5 ml and refreshed twice a week after that. Fibroblasts growing from the biopsy pieces were maintained in Dulbecco's Modified Eagle Medium (Gibco, France; Thermo Fisher Scientific, France) supplemented with 10% fetal bovine serum Good (PAN-Biotech, Aidenbach, Germany), 1% NEAA (Gibco, France), 1%

penicillin/streptomycin (Gibco, France), 1% kanamycin (Gibco, France) and 0.1% amphotericin B (Gibco, France) and incubated in a humidified incubator at 37°C with 5% CO_2.

Redox status analysis

Redox status was analyzed by measuring ROS levels with dihydrorhodamine 123 which is a reactive oxygen species (ROS) indicator that is oxidized to cationic rhodamine 123 in mitochondria and thus exhibits fluorescence. When indicated, fibroblasts were analyzed after zenital UV exposure (7.4 J/cm^2, 18 mins) at 80% confluency as positive controls. Transfected fibroblasts and controls were trypsinized and then incubated for 30 min in dark at 37°C, 5% CO_2 with 5µM of dihydrorhodamine 123. Cells were then centrifuged and resuspended in PBS for the analysis by an Epics XL-MCL flow cytometer (Beckman Coulter, USA).

Lentiviral-based shRNA transduction

For shRNA transduction of human dermal fibroblasts, plasmids purchased from Sigma-Aldrich (USA) were packaged into lentiviral particles by the lentivectors production facility from the SFR Biosciences Gerland (UMS 3444/US8, Lyon Sud, France). Five shRNA against NRF2 were first tested in primary fibroblasts to select the best shRNA sequence with the highest knock-down efficacy in our system to conduct further experiments. Primary papillary fibroblasts from one of the female donors previously described, were transduced at a 60% stage of confluency with highly concentrated shNrf2 or shCtrl lentiviral particles at the multiplicity of infection (MOI) of 5, with 8 µg/ml of polybrene for 8h. The infection was then stopped and cells were left in the incubator to recover with fresh cell culture media during 40h. Cell sorting was then performed using a BD FACSAria™ III flow cytometer (BD Biosciences, USA) to enrich the population of cells with the RFP-positive transduced cells. Population enriched either with shCtrl or shNrf2 transduced fibroblasts were further cultivated through 2 passages. These

passages allow them to recover a normal doubling time. shCtrl and shNrf2 fibroblasts were finally harvested for cell banking at the end of passage 6 (P6). Fibroblasts were then thawed at the beginning of each experiment to perform the different analyses at P7.

RT-qPCR analysis

Total RNA extractions were performed using the RNeasy kit (Qiagen, Germany), including a DNAse treatment, according to the manufacturer's instructions. RNA concentration and quality were assessed using NanoDrop 2000 (Thermo Fisher Scientific, France). cDNA was then synthesized using the iScript cDNA Synthesis kit (Bio-Rad, USA) with 500 ng of total RNA according to manufacturer's instructions. Reverse transcription quantitative real-time PCR (RT-qPCR) primers were either manually designed to obtain amplicons between 100 and 150 bp or the QuantiTec primers purchased from Qiagen (Germany). RT-qPCR primers used are listed in Supplementary Table S5. qPCR was performed according to the manufacturer's instructions using the iTaq Universal SYBR Green Supermix (Bio-Rad, USA) and a CFX96 Real Time PCR detection system (Bio-Rad, USA). Data were finally analyzed using the ΔΔCt method and normalized to three housekeeping genes *RPLP0*, *HPRT1* and *PPIB*.

For BCS dermal fibroblast cultures and controls, after RNA extraction performed as described above, cDNA was synthesized from 1 µg of mRNA using the iScript cDNA synthesis kit (Bio-Rad, USA) followed by RT-qPCR using 10 ng input cDNA and the SsoAdvanced Universal SYBR Green Supermix (Bio-Rad, USA) according to the manufacturer's instructions on a LightCycler®480 instrument (Roche Life Science, Germany). Data analysis was performed with the qBasePlus software (Biogazelle, Ghent, Belgium) using the three housekeeping genes *HPRT1*, *YWHAZ* and *RPL13A* for normalization. RT-qPCR primers used are listed in Supplementary Table S5.

RNA sequencing and data analysis

Concentration and quality of the RNA samples were assessed using Qubit 2.0 (Thermo Fisher Scientific, France) and TapeStation 2200 (Agilent Technologies, France), respectively. All RNA samples used in this study were of high quality with RNA Integrity Number (RIN) higher than 9.4. Barcoded libraries were built using SENSE mRNA-seq Library Prep Kit V2 (Lexogen) following the manufacturer's instructions. Libraries were pooled in equimolar ratios and sequenced on Illumina NextSeq 500 sequencing platform in single end (75 bp). At least 35 million reads per sample were obtained. AltraBio company (Lyon, France) performed the data analyses and generated the results in a friendly format under their proprietary interactive tool, WikiBioPath. Roughly, reads were mapped to the human reference genome GRCh38.p12 using STAR (Dobin et al., 2013). Then, differential gene expression (DGE) analysis was performed using DESeq2 package (Anders and Huber, 2010) with a filtering step (genes that did not have more than 0.339 count per million counts in at least 2 samples were filtered out) and corrections (to remove library size and technical effects).The differentially expressed (DE) genes were further analyzed considering various thresholds. Only DE genes with adjusted p-value <0.05 were considered as significantly expressed. The fold change was computed as the ratio of mean expression for siNrf2 and siCtrl conditions (siNrf2/siCtrl). Reciprocal ratio was taken for values lower than 1 and reported as negative. Significant DE genes with absolute fold change either > x2 or < /2 and ≥ x1.4 or ≤ /1.4 were considered for further investigations and according to the analyses. The GOrilla web tool (http://cbl-gorilla.cs.technion.ac.il/) was used to identify enriched Gene Ontology (GO) terms of the Biological Process category for the significant DE genes. Finally, the functional enrichment analysis (protein-protein interaction networks) was realized using the online STRING database v11.0 (https://string-db.org/).

Western blotting

Total proteins were extracted by scraping fibroblasts cell culture on ice, in RIPA lysis buffer (Sigma-Aldrich, USA) supplemented with Halt Protease & Phosphatase inhibitor cocktail (Thermo Fisher Scientific, France). Cell lysates were then left at 4°C for 30 min and centrifuged at 15000 rpm at 4°C during 15 min. Supernatants were collected and protein concentrations were assessed using the BCA protein assay kit (Thermo Fisher Scientific, France). 10 µg of proteins were separated on a 10% precast PROTEAN® TGX™ gel (Bio-Rad, USA) and then transferred to a PVDF membrane (Merck Millipore, Germany) overnight at 4°C. Membranes were then saturated during 1h at room temperature (RT) and incubated with the primary antibodies: NRF2 rabbit polyclonal antibodies (1:400, PA5-27882, Thermo Fisher Scientific, France), NQO1 monoclonal mouse antibody (1:500, sc-32793, Santa Cruz, US). For extracellular matrix protein immunodetection, membranes were incubated with rabbit polyclonal antibodies to collagen I (1:700, 20111, Novotec, France), periostin (1:2000, 20302, Cell Signaling, USA), fibrillin-2 (1:2000; ab128026, Abcam, France) and elastin (1:8000, 25011, Novotec, France) or monoclonal antibody to human collagen V (1:1000, 18G5; Bonod-Bidaud et al, 2007). Immunological detection was performed using anti-rabbit or anti-mouse HRP-coupled secondary antibodies (1/10000, Bio-Rad, USA), Clarity™ or Clarity Max™ Western ECL substrate (Bio-Rad, USA) and a ChemiDoc MP system (Bio-Rad, USA) for membrane imaging and analysis. When needed, membranes were stripped by incubating with the Antibody Stripping buffer (Gene Bio-Application L.T.D, Germany) during 30 min at RT. Immunodetection of GAPDH (1:1000, 2118S, Cell Signaling Technologies, USA) and TGX stain free images were used as loading controls and for densitometric quantification. Signal quantification was performed using ImageJ software.

Immunofluorescence staining and quantification

Human skin papillary fibroblasts were fixed with 4% paraformaldehyde (Thermo Fisher Scientific, France) and permeabilized with 0.1% Triton X-100 (Sigma-Aldrich, USA). After blockage in 3% bovine serum albumin (BSA) (Sigma-Aldrich, USA), cells were incubated with primary antibodies, rabbit polyclonal antibodies to human collagen I (1/200, Novotec, France) or home-made monoclonal antibody to human collagen Vα1 (1/800, Bonod-Bidaud et al., 2012), followed by incubation in Alexa Fluor 488 coupled secondary antibodies (1/1000, Thermo Fisher Scientific, France) and Hoechst solution (Invitrogen, USA). Cells were mounted in Dako fluorescent mounting medium (Agilent Technologies, France). Quantification of intracellular and extracellular collagen I and V immunofluorescence was performed using Fiji software. Two or 3 brighter Z plane was selected and assemble by "Z project" Fiji command. The entire field was selected and integrated density, area and mean fluorescence of collagen I or V staining were measured, with one area background measurement. Using these measures, the total corrected fluorescence [integrated density − (area of all selected picture × mean fluorescence of background measures)]/number of nuclei was calculated with Fiji macro. Measurements were performed on images from 3 independent experiments and about 20 fields for each condition.

BCS and healthy human fibroblasts fixed with 4% (w/v) paraformaldehyde (PFA; Sigma-Aldrich, USA) after 4 days of culture, and permeabilized with 0.5% (v/v) Triton X-100 in 1× phosphate buffered saline (PBS; Sigma-Aldrich, USA) for staining of intracellular proteins. After blocking with 5% BSA (in PBS; Sigma-Aldrich, USA) samples were incubated with a primary antibody against collagen I (1/25, Merck Millipore, Germany). Bound primary antibody was detected with Alexa Fluor 488 conjugated secondary antibody (1/1500, Molecular Probes, Life Technologies Europe). Antibodies were diluted in a 2% BSA/PBS (w/v) solution. Nuclei were counterstained with 4′-6-diamidino-2-phenylinodole hydroxychloride (DAPI;

Molecular Probes, Life Technologies Europe). Quantification of intracellular collagen I immunofluorescence was performed using Fiji software. An outline was drawn around the staining (comprising mainly endoplasmic reticulum and Golgi apparatus) and integrated density, area and mean fluorescence of collagen I staining were measured, along with five adjacent background measures. Using these measures, the total corrected fluorescence [integrated density − (area of selected staining × mean fluorescence of background measures)] was calculated. This process was repeated on a total of 50 different cells.

TEM analysis

Human dermal fibroblasts (transduced fibroblasts or BCS) were fixed in 2% PFA and 2.5% glutaraldehyde diluted in 0.2 M cacodylate buffer (pH 7.4) 20 min at RT and then overnight at 4°C. Samples were then washed with 0.2 M cacodylate buffer (pH 7.4) (5 min, 3 times). After post-fixation in 1% osmium tetroxide in 0.1 M cacodylate buffer, samples were gradually dehydrated in successive baths of ethanol (from 30% to 100%) and embedded in epoxy resin. 70nm-ultra-thin sections of shCtrl and shNrf2 fibroblasts cultures were performed and stained with 7% uranyl actetate in methanol and lead citrate before observation.

AFM analysis

For decellularization, shCtrl and shNrf2 fibroblasts were cultivated for 8 days in a cell culture medium supplemented with 1 mM Vitamin C (Sigma-Aldrich, MO, US) in 35 mm Petri dishes (3 dishes/condition). Samples were washed three times in PBS and then decellularized using the following lysis solution: 0.5% Triton X-100 and 20 mM NH_4OH in PBS during 5 min at RT. Lysis was followed under the microscope and stopped by adding gently 3 ml of PBS. Samples were washed three times with PBS, fixed in a 4% paraformaldehyde solution (Thermo

Fisher Scientific, France) during 1h at RT and then conserved at 4°C in PBS until measurements.

For AFM measurements, the PeakForce QNM (Quantitative Nanomechanical Mapping) AFM mode was used. The foundation of material property mapping with PeakForce QNM is the ability of the system to acquire and analyze the individual force curves from each tap that occurs during the imaging process. The spring constant of the cantilever used was of 0.37 N/m with a radius <10nm, according to the manufacturer. The deflection sensitivity of cantilevers was calibrated against a clean silicon wafer. AFM pictures were acquired with a cantilever with a spring constant of 6 N/m. Storage modulus G (elastic response) measurements were made in 1× PBS at room temperature and AFM pictures were acquired on dried samples. Storage or elastic modulus G, also known as Young's modulus, measures the mechanical properties (stiffness) of the ECM produced by the fibroblasts.

***In silico* analysis**

DNA sequences of proximal promoters of *NFE2L2* target genes (-1500/+100 bp from the transcription start site (TSS)) were obtained from R Bioconductor packages TxDb.Hsapiens.UCSC.hg19.knownGene, GenomicFeatures and Biostrings. Sequences were scanned for matches to human *NFE2L2* motifs (MA0150.1, JASPAR database http://jaspar.genereg.net/) using the MEME-FIMO on-line tool (http://meme-suite.org/tools/fimo).

ChIP-seq data targeting *NFE2L2* in human IMR-90 cells were downloaded from the ENCODE data portal (https://www.encodeproject.org/) (ENCODE Project Consortium, 2012, project GSE91565 in the NCBI-GEO database) GRCh38 genome, ENCFF474PPT file giving optimal IDR thresholded peaks, IDR<0.05). Annotation of the 17,298 peaks was made the R package ChIPseeker leading to 8932 genes associated with *NFE2L2* ChIP-seq peaks.

SUPPLEMENTARY FIGURES

Figure S1: NRF2 silencing in human skin papillary fibroblasts (siNRF2). (**a**) Representative bright field images of human dermal fibroblasts at 72h post-transfection. Scale bars = 100µm. (**b**) qRT-PCR analysis of *NFE2L2*, *NQO1, SLC7A11* at 72h post-transfection. Statistics were performed using the ordinary one-way ANOVA test (n_donor = 3, in duplicate). Asterisks indicate p-value: ***≤ 0.001, ns: non-significant. Errors bars represent mean ± SEM. (**c**) Western blots with anti-NRF2 and anti-NQO1 antibodies of total protein extracts of fibroblasts 72h after transfection. Representative membranes are shown (one donor among the 3). NT: non-transfected; siCtrl: non-targeting siRNA; siNrf2_1 and siNrf2_2: NRF2 targeting siRNAs. NT and siCtrl are controls.

Figure S2: Bioinformatics analysis of siNrf2 fibroblasts transcriptome. (**a**) Principal component analysis of the transcriptomic data. (**b**) Volcano plots of differentially expressed genes in siNrf2 (NRF2-targeting siRNA) *vs* siCtrl (non-targeting siRNA) fibroblasts. Green dots correspond to significant differentially expressed genes (fold change ≥ 2; p-value <0.05) and grey dots are not significantly expressed genes. Named genes are NRF2 conventional (antioxidant and metabolic) targets already described in literature. (**c**) Top downregulated target genes NRF2 (FC ≤ -6; p-value set at 0.05). (**d**) Gene Ontology (GO) enrichment analysis of differentially expressed genes in both siNrf2.

Figure S3: Redox status of siNrf2 fibroblasts. (a) Intracellular ROS level measurements in transfected human dermal fibroblasts 72 hours after transfection determined by a flow cytometry method using dihydrorhodamine 123 (DHR) free radical sensor. HDF (donor 1) were treated or not with zentithal UV (7.4 J/cm^2, 18 mins) as a positive control of ROS measurement. (b) List of differentially gene expression of the ROS system extracted from siNrf2 fibroblasts RNAseq data.

NT: non-transfected; siCtrl: non-targeting siRNA; siNRF2_1 and siNrf2_2: NRF2-targeting siRNAs. NT and siCtrl are controls.

Figure S4: Generation of a stable human dermal fibroblast line silenced for NRF2 (shNrf2). (a) Timeline of the protocol used to generate the shCtrl and shNrf2 fibroblast lines. shCtrl: non-targeting shRNA; siNrf2_2: NRF2-targeting shRNA. (b) Bright field images of the cells before and after transduction. Scale bars = 100µm. (c) Percentage of transduced fibroblasts after transduction (upper line) and after cell sorting (lower line) determined by flow cytometry. (d) qRT-PCR analysis of NRF2 and its conventional antioxidant targets genes in shCtrl and shNrf2 fibroblasts. Statistics were done using a paired t-test (n_experiments = 3). Asterisks indicate p-value: * ≤ 0.05, ** ≤ 0.01. Errors bars represent mean ± SEM. (e) Western blots with anti-NRF2 and anti-NQO1 antibodies of total protein extracts from shCtrl and shNrf2 fibroblasts.

Figure S5: Atomic force microscopy (AFM) analysis of shNrf2 decellularized ECM. (**a**) AFM images showing the topography of decellularized matrices secreted by shCtrl (upper panel) and shNrf2 (lower panel) fibroblasts. ECM empty spaces are marked with white dotted circles. Scale bars = 20µm. (**b**) Storage modulus G' measurements (in kPa) of shCtrl and shNrf2 decellularized matrices (10,000 measurements were acquired per areas, 7 and 8 areas of 3 independent shCtrl and shNrf2 samples were analysed, respectively). Storage modulus G' (also known as Young's modulus) values reflect the stiffness of the ECM network produced by the fibroblasts. Histogram shows average values for each area. Statistics were done using a non-paired t-test; n_areas = 7 for shCtrl and shNrf2. Asterisks indicate p-value: * ≤ 0.05, ** ≤ 0.01, ***≤ 0.001, ns: non-significant. shCtrl: non-targeting shRNA; siNrf2_2: NRF2-targeting shRNA.

Figure S6: Densitometric quantification of ECM expression levels in shCtrl and shNrf2 fibroblasts cell layers: collagen I (ColIα1), collagen V (ColVα1), periostin, elastin and fibrillin-2 expression levels. Western blot membranes are probed with anti-collagen I, anti-collagen V, anti-periostin and anti-elastin as indicated. Histograms show quantification of protein signal using total loading (TGX stain-free images) or GAPDH as loading controls. For fibrillin-2, the ~200kDa protein signal was used for quantification. Statistics were performed using Student's t-test. Errors bars represent mean ± SEM; n = number of membranes analyzed. Asterisk indicates p-value: * ≤ 0.05, *** ≤ 0.001; ns, non-significant (p-values are indicated in brackets).

Figure S7: Immunofluorescence staining of intracellular collagen I in BCS skin fibroblasts. (**a**) Immunofluorescence staining of the intracellular collagen I in human skin fibroblasts from one control donor (Ctrl) and two BCS patients with *ZNF469* mutations (P1 and P2) at 4 days after seeding. Scale bars = 50µm (**b**) Quantification of collagen I intracellular immunofluorescence intensity. Statistics were performed using the ordinary one-way ANOVA test. Asterisks indicate p-value: ***≤ 0.001, * ≤ 0.05, ns: non-significant. Errors bars represent mean ± SEM.

SUPPLEMENTARY TABLES

Supplementary Table S1: List of genes differentially expressed conventional antioxidant and metabolic targets of NRF2 in siNrf2_1 and siNrf2_2 compared to controls. Genes have been considered as significantly differentially expressed when the fold change ≥ 2 and the p-value <0.05.

Supplementary Table S2: List of differentially expressed matrisome genes in siNrf2 human dermal fibroblasts. Fold change ≥1.4; p-value <0.05. Genes in bold are also dysregulated in mouse fibroblasts with constitutively activated expression of Nrf2 (Hiebert et al, 2018). When underlined they show the expected opposite direction in expression.

Supplementary Table S3: List of siRNAs and shRNAs used in the study. **a**, list of siRNAs; **b**, list of shRNAs**.** shCtrl does not target any known gene. The selected shRNAs are in bold.

Supplementary Table S4: List of RT-qPCR primers. Sequences or supplier reference are provided.

Supplementary Figure S1

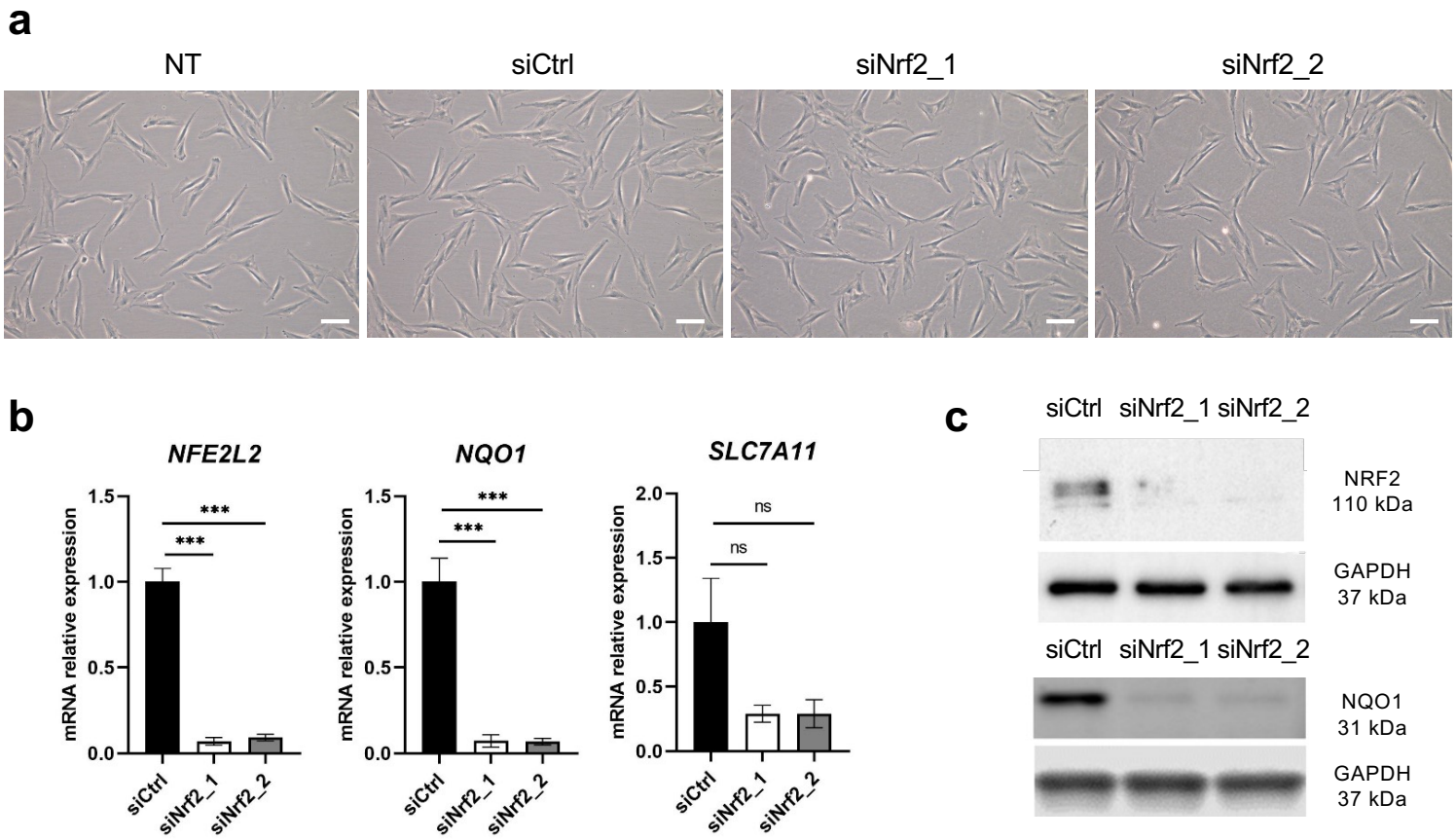

Supplementary Figure S2

a

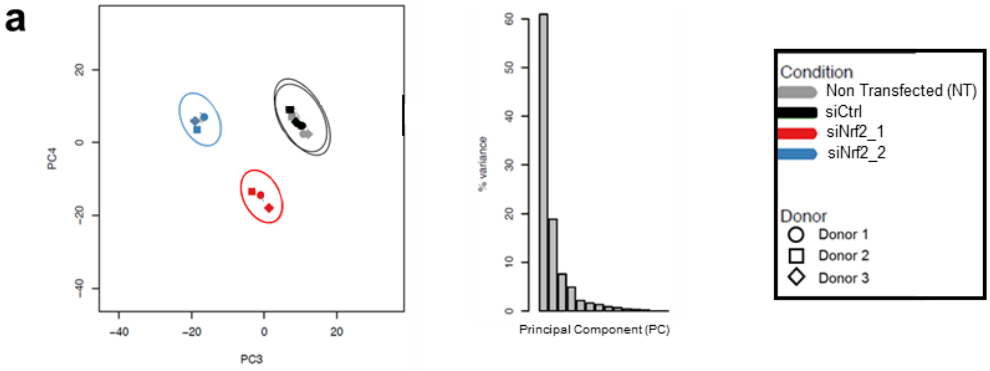

b

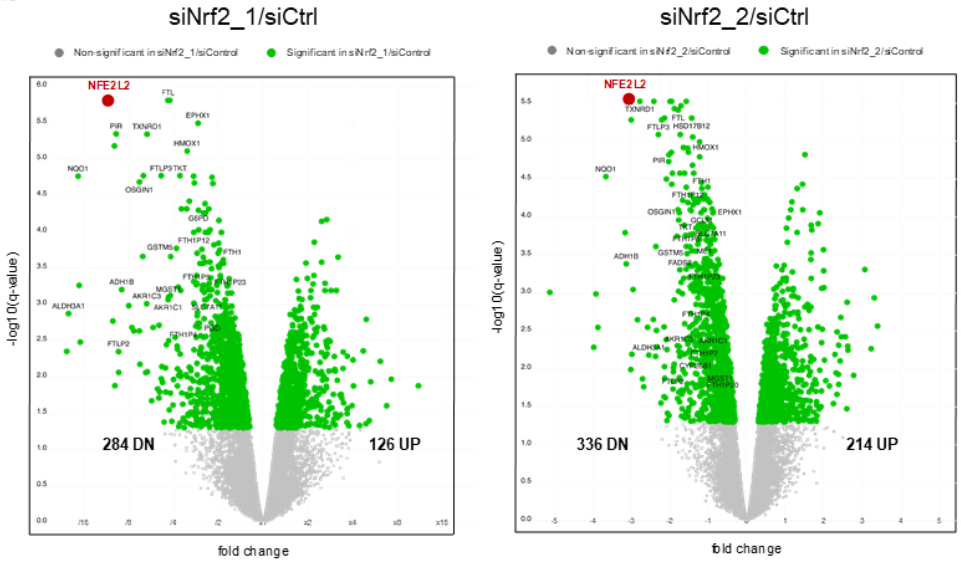

c

Top downregulated NRF2 antioxidant and metabolic genes	Fold change in siNrf2_1 and 2 vs. siCtrl	
ADH1B	-8.885	-8.751
AKR1C3	-6.040	-3.375
ALDH3A1	-20.211	-5.828
AMBP	-9.878	-15.710
FTLP2	-9.326	-3.777
NFE2L2	-10.791	-8.55
NMRAL2P	-20.763	-14.573
NQO1	-17.412	-12.629
PIR	-9.686	-4.072
TRIM16	-6.357	-3.448
TRIM16L	-9.941	-8.001
TXNDR1	-6.001	-6.854

d

Description	GO Term	FDR	Number of genes from our data in the GO Term Relatively to the103 common genes in the 2 siNrf2
Detoxification	GO:0098754	1.74E-3	7
Cellular metal ion homeostasis	GO:0006875	2.49E-3	11
Chemical homeostasis	GO:0048878	3.38E-3	15
Metal ion homeostasis	GO:0055065	3.9E-3	11
Cellular homeostasis	GO:0019725	4.32E-3	13
Cellular detoxification	GO:1990748	1.71E-2	5
Regulation of retinoic acid receptor signaling pathway	GO:0048385	3.59E-2	3
Negative regulation of growth	GO:0045926	4.23E-2	7

Supplementary Figure S3

a

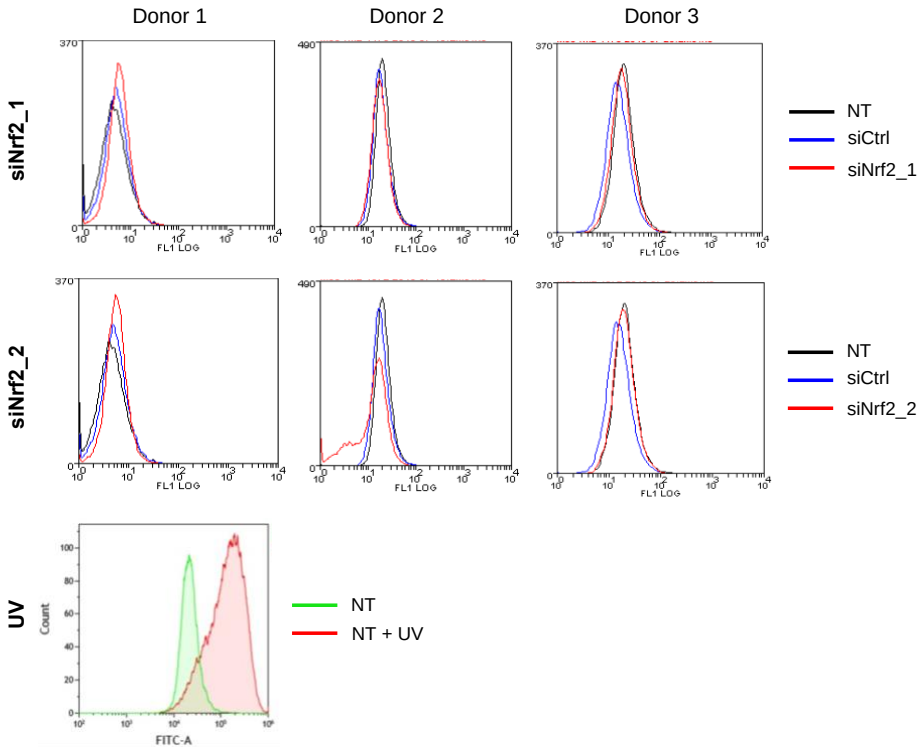

b

ROS Genes References		Fold change in siNrf2_1 and 2 vs. siCtrl (p-value)	
St Pierre *et al.*, 2006	*CAT*	1.096 (0.419)	-1.103 (0.397)
	PPARGC1A	-1.026 (0.963)	-2.676 (0.0685)
	SOD1	1.268 (0.134)	1.207 (0.242)
	SOD2	-1.121 (0.550)	1.072 (0.728)
	SOD3	-1.798 (0.0128)	-1.481 (0.0644)
	GPX1	-1.156 (0.253)	-1.178 (0.209)
Spadoni *et al.*,2015 Murphy-Mashman *et al.*, 2017	*NOX4*	1.174 (0.537)	1.5 (0.0929)
	NOX5	1.280 (0.634)	1.656 (0.268)

Supplementary Figure S4

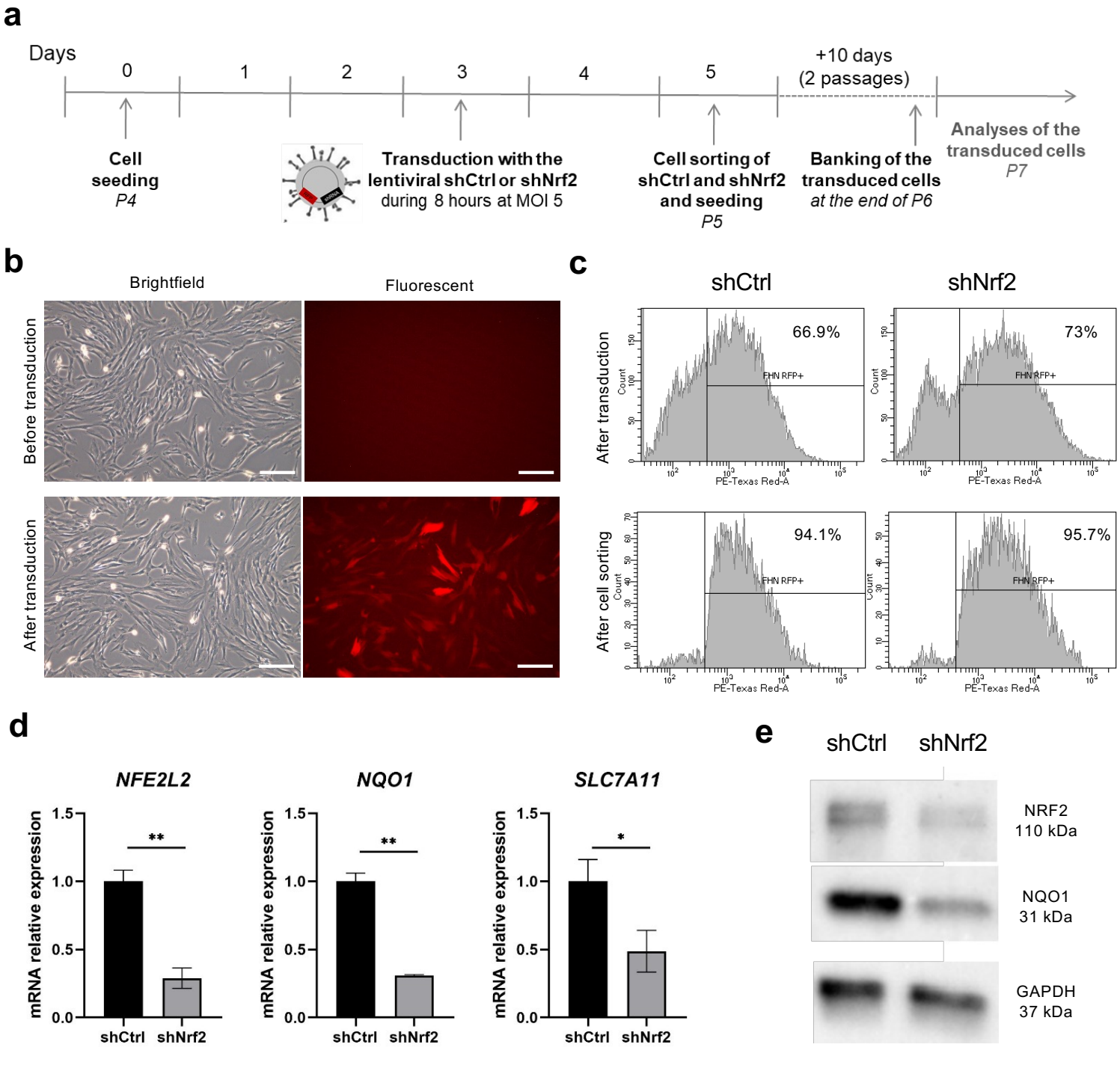

Supplementary Figure S5

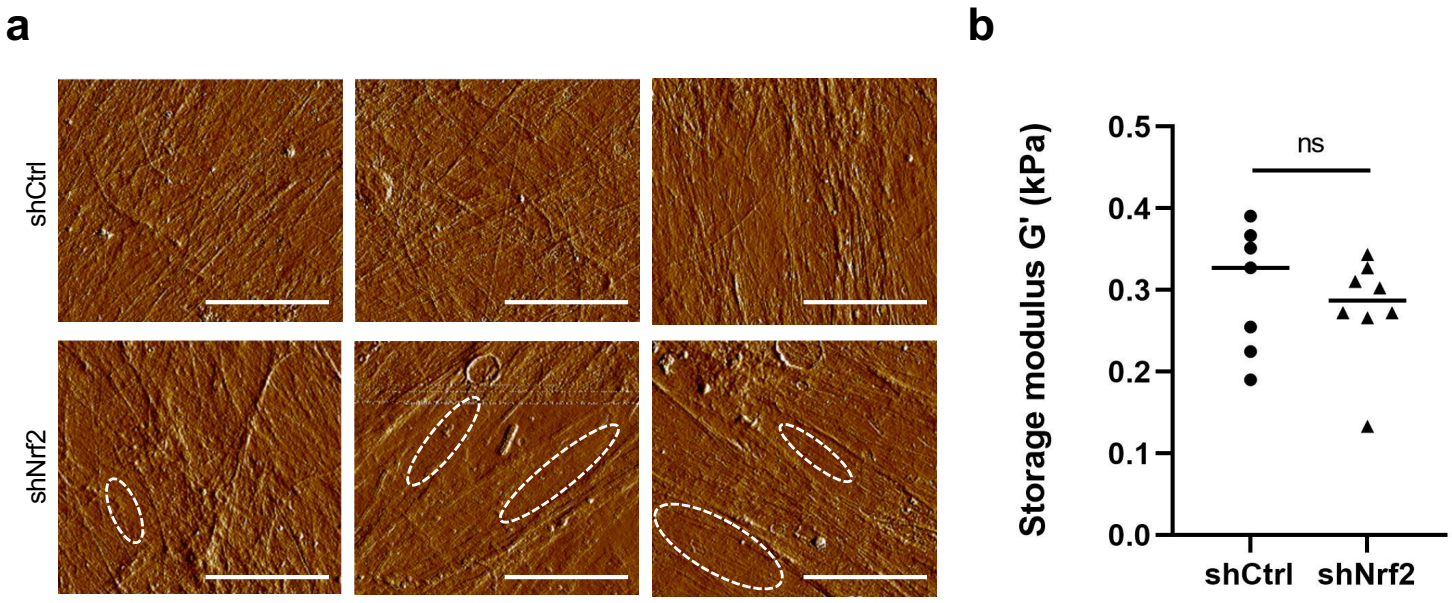

Supplementary Figure S6

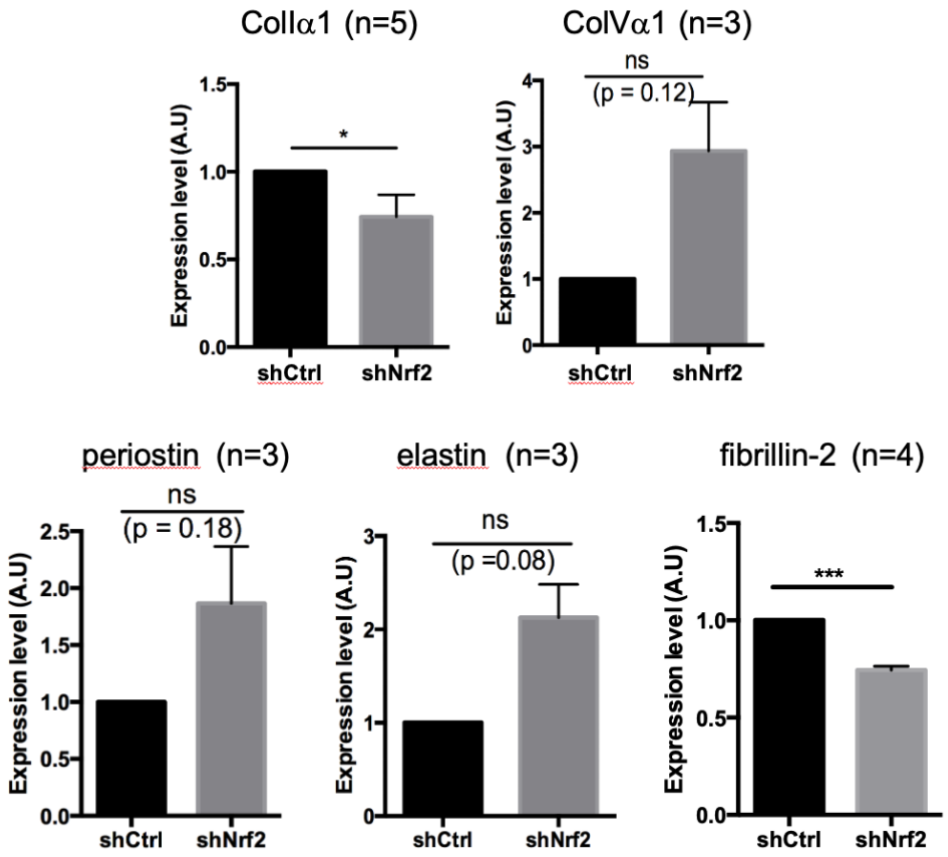

Supplementary Figure S7

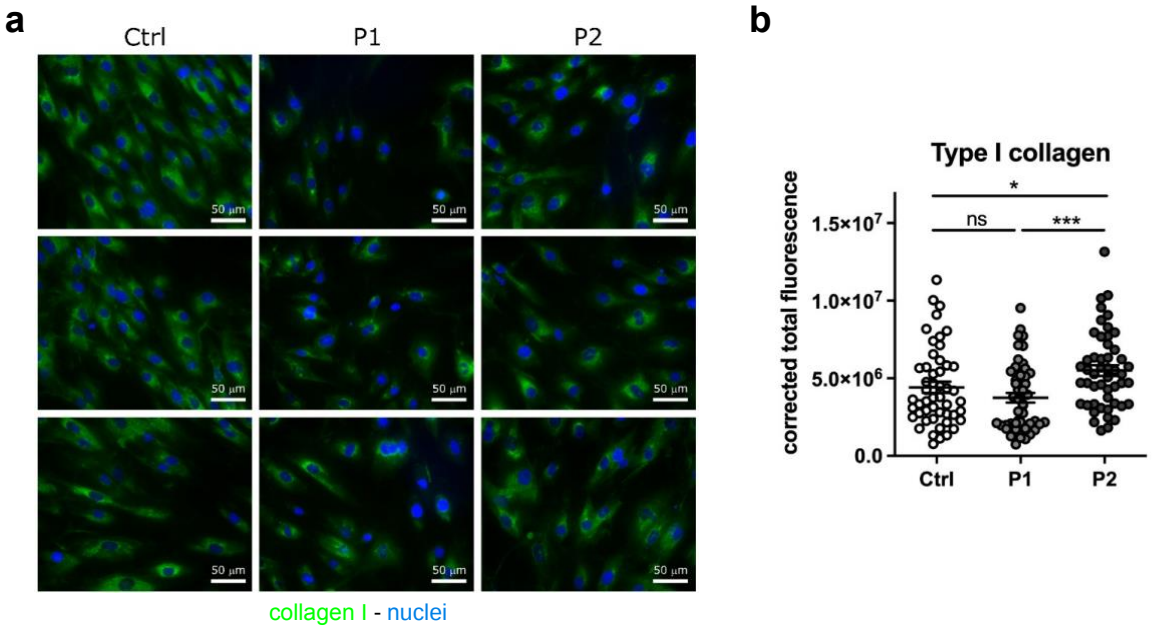

Supplementary Table S1

NRF2 function categories	Gene	Fold change siNrf2_1/siControl	Fold change siNrf2_2/siControl
	NFE2L2	-10.791	-8.550
Detoxification: phase I and II proteins	*ADH1B*	-8.885	-8.751
	AKR1C1	-4.336	-2.590
	AKR1C2	-4.523	-2.267
	AKR1C3	-6.040	-3.375
	ALDH3A1	-20.211	-5.828
	ALDH4A1	-2.064	-1.234
	CYP26B1	-3.066	-2.513
	CYP27B1	1.233	2.509
	CYP7B1	-2.286	-1.371
	EPHX1	-2.729	-1.841
	NMRAL2P	-20.763	-14.573
	NQO1	-17.412	-12.629
	MGST1	-4.300	-2.216
Heme and iron metabolism	*AMBP*	-9.878	-15.710
	FTH1	-2.002	-2.244
	FTH1P10	-1.155	-2.132
	FTH1P11	-1.740	-2.042
	FTH1P12	-2.914	-2.886
	FTH1P20	-2.010	-2.242
	FTH1P23	-2.296	-2.139
	FTH1P3	-1.437	-2.281
	FTH1P4	-2.615	-2.494
	FTH1P5	-2.806	-2.965
	FTH1P7	-1.905	-2.142
	FTL	-4.346	-3.435
	FTLP2	-9.326	-3.777
	FTLP3	-4.825	-4.904
	HMOX1	-3.227	-2.895
	PIR	-9.686	-4.072
Carbohydrate metabolism and NADPH regeneration	*G6PD*	-2.709	-1.980
	ME1	-1.829	-2.135
	PGD	-2.190	-1.644
	TKT	-3.611	-2.494
Lipid metabolism	*ACOT4*	-2.018	-1.067
	FADS2	-1.979	-2.520
Antioxidant : Glutathione metabolism	*GCLM*	-1.775	-2.256
	GSTM5	-3.810	-2.926
	SLC7A11	-2.382	-2.757
Antioxidant : TXN based system	*TXNRD1*	-6.001	-6.854
Proteostasis	*SQSTM1*	-2.197	-1.554
	TRIM16	-6.357	-3.448
	TRIM16L	-9.941	-8.001

Supplementary Table S2

Matrisome Categories	Gene	Fold change in siNrf2_1 and 2 vs. siCtrl		
Collagens	*COL24A1*	-4.61	-4.67	DOWN
	COL1A2	-1.46	-1.45	DOWN
	COL1A1	-1.38	-1.47	DOWN
	COL10A1	4.7	3.2	UP
ECM Glycoproteins	***FBN2***	-2.79	-1.49	DOWN
	NTN1	-2.52	-1.57	DOWN
	IGSF10	-1.67	-1.83	DOWN
	FNDC1	-1.52	-1.55	DOWN
	SVEP1	-1.61	-2.67	DOWN
	ELN	1.52	1.72	UP
	COMP	1.81	1.50	UP
	POSTN	1.55	1.65	UP
Proteoglycans	***ESM1***	3.16	8.37	UP
ECM regulators	*AMBP*	-9.88	-15.71	DOWN
	MASP1	-1.55	-3.87	DOWN
	TIMP3	1.56	2.05	UP
	ADAMTS4	1.71	2.18	UP
	TGM2	2.38	2.00	UP
Secreted factors	*PIK3IP1*	-1.50	-2.15	DOWN
	WNT2	-1.58	-1.67	DOWN
	CCL2	-1.96	-1.90	DOWN
	FGF13	-1.91	-1.83	DOWN
	ANGPTL2	-1.42	-2.17	DOWN
	CXCL3	-7.97	-4.43	DOWN
	IL15	-1.74	-1.82	DOWN
	PDGFD	-1.67	-2.06	DOWN
	CCBE1	-1.49	-1.41	DOWN
	IL11	1.99	1.91	UP
	HBEGF	2.23	1.64	UP
	LIF	3.11	2.38	UP
	ANGPTL4	2.52	2.70	UP
ECM-affiliated proteins	***GPC1***	-1.75	-1.55	DOWN
	SEMA3A	-1.54	-2.12	DOWN
	COLEC12	-1.65	-1.68	DOWN
	CLEC3B	-1.79	-1.48	DOWN
	CLEC2D	1.96	1.84	UP
	SEMA7A	2.09	2.01	UP

Supplementary Table S3

a

siRNA name	siRNA sequence (5' to 3')
siNrf2_1	CAAGCUGGUUGAGACUACCAUGGUU
siNrf2_2	CAAUGAUUCUGACUCCGGCAUUUC
siKeap1	UGUGUGACGUCACACUGCAGGUCAA
siZNF469_1	CCGAGGGUGCAGUCCUGCUAGAGAA
siZNF469_2	CAGGAACUUUCAUUUCCUAAGAAUA

b

	Mission® Custom Plasmid TRCN number	DNA sense sequence (5' to 3')	Vector
shCtrl	**Non Target shRNA**	**GCGCGATAGCGCTAATAATTT**	pLKO.1-U6-shRNA-CMV-TAGRFP
shNrf2 - 1	**TRCN0000284998**	**GCTCCTACTGTGATGTGAAAT**	
shNrf2 - 2	TRCN0000273552	CTTGCATTAATTCGGGATATA	
shNrf2 - 3	TRCN0000284999	CCGGCATTTCACTAAACACAA	
shNrf2 - 4	TRCN0000007556	GCACCTTATATCTCGAAGTTT	
shNrf2 - 5	TRCN0000273494	AGTTTGGGAGGAGCTATTATC	

Supplementary Table S4

Experiments	Gene	Forward primer (5' to 3')	Reverse primer (5' to 3')
Human skin papillary fibroblasts	*NFE2L2*	GCAACAGGACATTGAGCAAG	TGGACTTGGAACCATGGTAGT
	NQO1	ACTGCCCTCTTGTGGTGCAT	GCTCGGTCCAATCCCTTCAT
	SLC7A11	GCGTGGGCATGTCTCTGAC	GCTGGTAATGGACCAAAGACTTC
	HMOX1	GCCTGGAAGACACCCTAATGTG	GGCCGTGTCAACAAGGATACTT
	COL1A1	CACTCCTTCCCAAATCTG	GAGCATTGCCTTTGATTG
	COL1A2	GAGGAGAGCCTGGCAACA	GGTCCCTGAGCACCATTG
	COL5A1	CCGGATGTCGCTTACAGAGT	CTGCCTTTCTTGGCTTTCAC
	PPIB	TGTGGTGTTTGGCAAAGTTC	GCTTCTCCACCTCGATCTTG
	HPRT1	GACCAGTCAACAGGGGACAT	CCTGACCAAGGAAAGCAAAG
	RPLP0	GTCACTGTGCCAGCCCAGAA	TCAATGGTGCCCCTGGAGAT
	ZNF469	QT00202566	
Skin fibroblasts from BCS patients	*COL1A1*	TCTCTGGCCTCCAGGGTC	GAGCACCAGCAGAGCCAG
	COL1A2	GACTGGTTTCCCTGGTGCT	CCCTTCTTTCCCAGCAGGA
	COL5A1	CGGGCCTTGCTGGAAAAGA	TCCTGGAGGGCCATCTTTC
	COL5A2	AGGTACCTCTGGTCCTCCT	TTCCCTTTTGGGCCAGCT
	ZNF469	ACGGAATGACAGACCCTGG	TCCCACTACCCTCGGTGG
	HPRT1	TGACACTGGCAAAACAATGCA	GGTCCTTTTCACCAGCAAGCT
	YWHAZ	ACTTTTGGTACATTGTGGCTTCAA	CCGCCAGGACAAACCAGTAT
	RPL13A	GAGCAAGGAAAGGGTCTTAG	ACTGGTTGCTCTTCCTATTG